Received: 29 May 2016 | Revised: 14 March 2017 | Accepted: 28 March 2017

DOI: 10.1002/gj.2935

WILEY

RESEARCH ARTICLE

Plagioclase crystallisation in a granodioritic melt and its petrogenetic implications for the origin of the A-type granite in East Junggar, NW China

Man Xu[1,2,3] | Hongfeng Tang[1]

[1] Key Laboratory for High Temperature and High Pressure Study of the Earth's Interior, Institute of Geochemistry, Chinese Academy of Sciences, Guiyang, China

[2] University of Chinese Academy of Sciences, Beijing, China

[3] Department of Earth, Environmental and Planetary Sciences, Case Western Reserve University, Cleveland, Ohio, USA

Correspondence
Hongfeng Tang, Key Laboratory for High Temperature and High Pressure Study of the Earth's Interior, Institute of Geochemistry, Chinese Academy of Sciences, Guiyang, 550081, China.
Email: tanghongfeng@vip.gyig.ac.cn

Funding information
Strategic Priority Research Program (B) of the Chinese Academy of Sciences, Grant/Award Number: XDB 18010401; National Natural Science Foundation of China, Grant/Award Number: 41172071

Handling editor: E. Bozkurt

Crystallisation experiments were performed on a natural I-type granodiorite from East Junggar of Xinjiang, NW China, at 1.0 and 1.5 GPa in the temperature range between 700 and 875 °C and for various water contents to investigate the crystallisation behaviour of plagioclase in granodioritic melts. Experimental results indicate that the optimal conditions for plagioclase to crystallise in this granodioritic melt are approximately 875 °C, 1.0 GPa, and ~10 wt% water content. All the experimental feldspars have ternary composition because of the high pressure in this study, with Or contents increasing while An contents decreasing with the increase of pressure. They consist of Or-rich plagioclase at 1.0 GPa, passing to An-rich alkali feldspars at 1.5 GPa. The ternary feldspar plays a role in keeping the total amount of alkali in the residual melt relatively constant. After plagioclase-dominant crystallisation, the residual melt shows characteristics similar to the A-type granites from East Junggar, implying that the fractional crystallisation of the I-type granodioritic melt at high pressure may be one of the important processes generating the A-type magmas in East Junggar. Mass balance calculation and trace element modelling show that the fractionally crystallised phase assemblage and proportion could be plagioclase (40.2 wt%) + orthopyroxene (6.3 wt%) + hornblende (6.3 wt%). The experimentally determined plagioclase crystal growth rates range from 1.17×10^{-8} to 2.70×10^{-8} mm/s. By comparing the crystal growth rate with the crystal size in natural rocks, the timescale of the crystallisation and differentiation of the I-type granodioritic magma that is parental to the A-type granitic magma in East Junggar was estimated to be several hundred years, in excellent agreement with the result from a simple numerical model.

KEYWORDS

A-type granite, East Junggar of Xinjiang, granodioritic melt, high-temperature and high-pressure experiments, NW China, plagioclase crystallisation

1 | INTRODUCTION

Plagioclase is one of the major rock-forming minerals in igneous rocks. Its crystallisation is of great significance to many geological processes: (a) The crystallisation of plagioclase can result in a remarkable change of the residual melt composition. For example, CaO and Al_2O_3 contents of the residual melt would decrease, and Eu, Sr, and Ba would show anomalies if plagioclase crystallises from the melt (Patiño Douce, 1997; Su, Tang, & Cong, 2008); (b) the intracrystalline diffusion of plagioclase is slow (Grove, Baker, & Kinzler, 1984; Morse, 1984), which makes it an ideal candidate to record the magmatic processes. As a result, we can use the texture of crystallised plagioclase (e.g., zoned texture and cellular texture) to reveal the kinetic processes of magma evolution (Loomis & Welber, 1982; Andersson & Eklund, 1994); (c) the physical and chemical conditions of magma formation can be investigated on the basis of the changes of the chemical composition of plagioclase and its elemental partitioning behaviour (Housh & Luhr, 1991; Wilke & Behrens, 1999; Aigner-Torres, Blundy, Ulmer, & Pettke, 2007; Mollo et al., 2011).

A number of researchers have investigated the crystallisation of plagioclase through high-temperature and high-pressure experiments because of the geological significance of plagioclase (e.g., Brugger & Hammer, 2010; Cabane, Laporte, & Provost, 2005; Couch, 2003; Larsen, 2005; Muncill & Lasaga, 1987, 1988; Orlando, D'Orazio,

 Copyright © 2017 John Wiley & Sons, Ltd.

Armienti, & Borrini, 2008; Simakin & Salova, 2004; Mollo et al., 2011). According to the experimental objectives and strategies, previous experimental studies concerning plagioclase crystallisation can be generally classified into four categories, as follows: (a) High-temperature and high-pressure experiments were used to simulate natural magmatic processes and to investigate the effect of melt composition, temperature, pressure, and water content on the crystallisation of plagioclase and the chemical composition of the crystallised plagioclase (e.g., Panjasawatwong, Danyushevsky, Crawford, & Harris, 1995; Takagi, Sato, & Nakagawa, 2005); (b) on the basis of the texture and morphology of experimentally crystallised plagioclase, researchers investigated the variations of magmatic conditions with time (e.g., Corrigan, 1982; Lofgren, 1974); (c) the kinetic processes of magma evolution were investigated through the crystal growth rate, chemical composition, and crystal size distribution analysis of experimentally crystallised plagioclase (e.g., Orlando et al., 2008); (d) element partitioning coefficients between plagioclase and coexisting melt were determined through experiments (e.g., Bindeman & Davis, 2000; Bindeman, Davis, & Drake, 1998).

Most of the aforementioned experimental studies on the crystallisation of plagioclase focused on basaltic systems. Plagioclase may fail to crystallise in experiments within granitic systems, even under large undercooling, because of the relatively high viscosity of granitic magmas (Gibb, 1974). As a result, less experiments have been conducted on granitic or granodioritic melts, and most of the previous experiments are phase equilibria studies (e.g., Bogaerts, Scaillet, & Auwera, 2006; Prouteau & Scaillet, 2003; Scaillet & Evans, 1999). To our knowledge, no study on plagioclase crystallisation under high pressure (~1.0 and 1.5 GPa) using natural granodiorite as the starting material has been conducted. As granodiorites are widely distributed all over the world and the average composition of the upper crust is similar to granodiorite (Rudnick & Gao, 2014), analysing the crystallisation behaviour in granodioritic system is important. It could help us better understand the variations of the chemical composition of the upper crust and the genesis of relevant rocks, such as the A-type granites occurring in East Junggar of Xinjiang, NW China, part of the well-known Central Asian Orogenic Belt. According to geochemical studies, several researchers suggest that the A-type granites were probably formed by fractional crystallisation dominated by plagioclase and hornblende of the granodioritic melt produced by partial melting of the oceanic crust in the Junggar orogen (Su et al., 2007; Tang, Qu, Su, & Cong, 2007; Zhao, Wang, Zou, & Masude, 1996). The fractional crystallisation of intermediate-acidic magmas to form rocks with A-type characteristics has also been reported in other regions. Jiang, Zhang, Zhou, and Liu (2009) investigated a Mesozoic granite with A-type characteristics from the North China Craton and concluded that the parental magmas of the granite were I-type and its A-type characteristics were the result of extensive fractionation. Hergt, Woodhead, and Schofield (2007) analysed an A-type suite from the Grampians region and concluded that the suite was formed by partial melting of the basement rocks and subsequently underwent variable fractional crystallisation dominated by hornblende and plagioclase. However, the hypotheses of these studies are based on geochemical data of the field samples, and their validities need the support from direct evidence of experimental petrology. As a result, conducting relevant experimental studies is of great significance.

In this study, a natural granodiorite sample collected from East Junggar was used as the starting material. Crystallisation experiments were performed on glass at 1.0 and 1.5 GPa between 700 and 875 °C for various water contents to investigate the following aspects: (a) the optimal conditions for plagioclase crystallisation in the granodioritic melt, (b) the plagioclase crystal growth rates in the natural granodioritic system, and (c) the experimental evidence for the petrogenesis of the A-type granites in East Junggar.

2 | EXPERIMENTAL AND ANALYTICAL METHODS

2.1 | Starting material

The natural I-type granodiorite (sample HY55) used in this study was collected from East Junggar, NW China. The sample is composed of plagioclase (42%), K-feldspar (23%), quartz (22%), hornblende (7%), and biotite (6%), with accessory opaques, zircon, and apatite. The experimental starting material was granodioritic glass produced by melting granodiorite twice at 1,500 °C and 1 atm with grinding between the two melting steps. The major element compositions of the glass determined by electron microprobe analysis (EPMA) are similar to those of the natural rock analysed through X-ray fluorescence spectrometer (Table 1).

2.2 | Experimental conditions and techniques

In nature, plagioclase can crystallise over a wide temperature range. Normally, the crystallisation temperature of plagioclase in felsic magmas ranges from 700 to 900 °C (Bogaerts et al., 2006; Dall'Agnol, Scaillet, & Pichavant, 1999; Klimm, Holtz, Johannes, & King, 2003; Klimm, Holtz, & King, 2008). Therefore, the experimental temperature was set from 700 to 875 °C in this study. Since the crystallised plagioclases are too tiny to analyse at 700–800 °C (see Figure 2), most of the experiments were carried out between 800 and 875 °C. The experimental pressure was set to 1.0 and 1.5 GPa, and the results of which could be applied to the investigation of the fractional

TABLE 1 Major element compositions of granodiorite and its glass as the starting material in this study

	SiO_2	TiO_2	Al_2O_3	$Fe_2O_3^*$	FeO*	MnO	MgO	CaO	Na_2O	K_2O	LOI	Total
HY55	64.89	0.52	15.12	4.54		0.07	1.64	3.41	3.86	3.08	1.24	98.37
Glass	64.92	0.58	15.75		3.23	0.08	1.49	3.68	4.26	2.87		96.86

Note. Fe_2O_3* and FeO* indicate that the total iron is expressed as Fe_2O_3 and FeO, respectively. The data for granodiorite (HY55) analysed through X-ray fluorescence spectrometer and its glass determined by electron microprobe analysis are from Su (2007) and Xia et al. (2010), respectively.

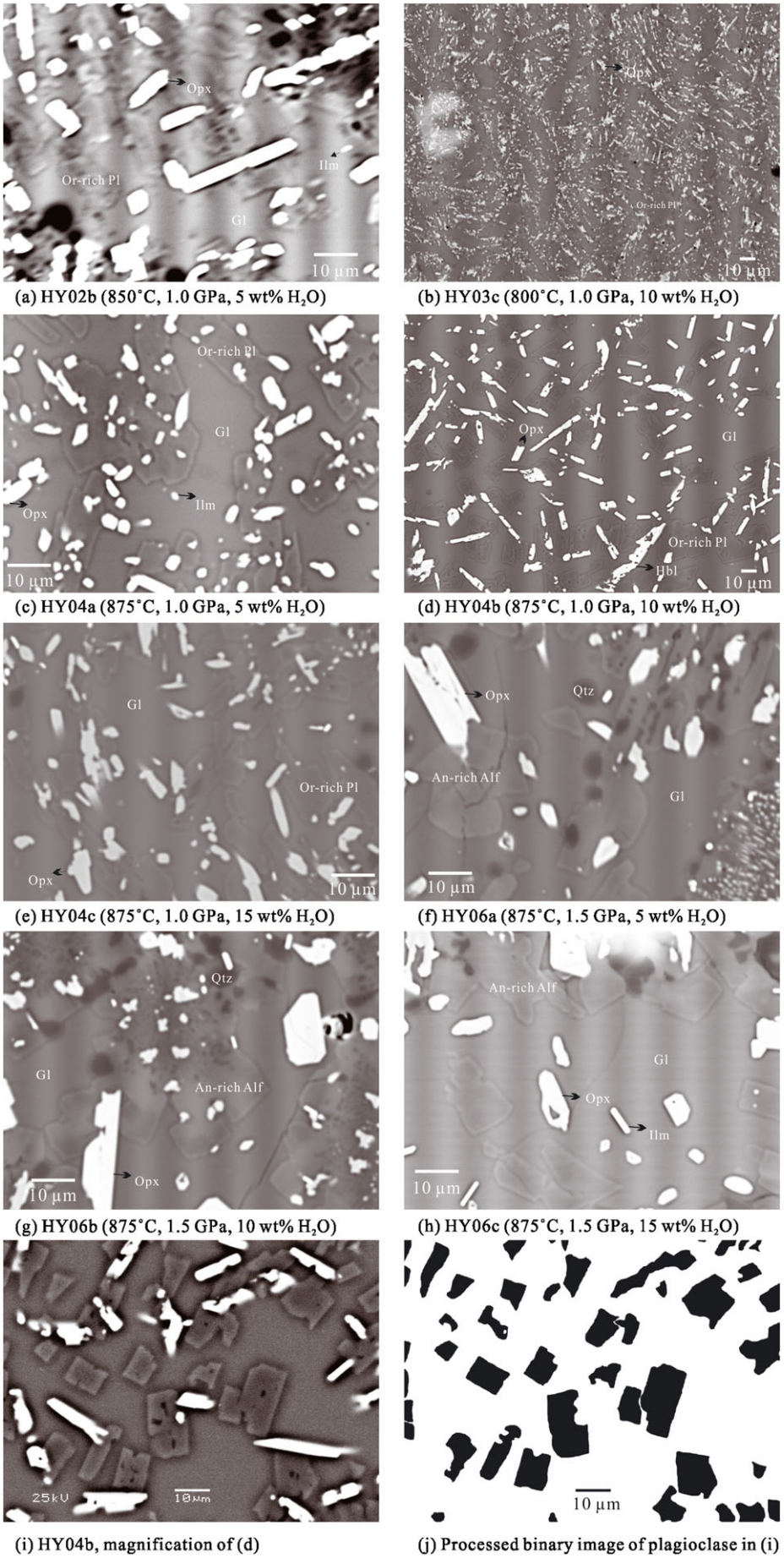

FIGURE 2 Representative images of the run products [Colour figure can be viewed at wileyonlinelibrary.com]

crystallisation of granodioritic magma in the lower continental crust. The added water contents in our experiments varied from 3 wt% to 15 wt% to investigate the influence of water on the crystallisation of plagioclase. The oxygen fugacity of the experiments was controlled by C–CO (CO_2)–O_2 buffering as a result of lining the graphite sleeve in the capsules, which provides a slightly reduced environment for the experiments. The detailed experimental conditions are listed in Table 2.

Crystallisation experiments were performed on the DS6*600t six-anvil apparatus equipped at the Key Laboratory for High Temperature and High Pressure Study of the Earth's Interior, Institute of Geochemistry, Chinese Academy of Sciences, Guiyang. The powered starting glasses were introduced into the platinum (Pt) capsule (7 mm in length and 3.5 mm in inner diameter). The detailed sample assembly is shown in Figure 1. The sample and the wall of the Pt capsule were separated by the graphite sleeve, which can prevent Fe loss (Sisson & Grove, 1993). The loaded capsules were welded by laser and checked for leakage at approximately 110 °C. Only those without water leakage were used in experiments. The prepared capsules were placed in a thin-walled Al_2O_3 sleeve. Then, the Al_2O_3 sleeve, together with the capsule, was placed in a graphite heater. The pressure transmitting medium in the experiments is pyrophyllite calcined at 800 °C. In a single run, the pressure was initially increased to the desired value. The uncertainty of the pressure was within 0.1 GPa. The charges were initially heated to 1,100 °C in two steps at a heating rate of approximately 35 °C/min for 40 min, to melt and homogenise the starting material, and then cooled down to the desired temperature at a cooling rate of approximately 2 °C/min for approximate 94 hr. Previous studies showed that a 94 hr crystallisation time was almost sufficient for the experiments to reach equilibrium under high water content conditions (Brugger, Johnston, & Cashman, 2003; Housh & Luhr, 1991). In addition, the crystallised plagioclases are euhedral or subhedral and are distributed evenly in the run products. The compositions of the residue melts are relatively homogeneous in our experiments. Consequently, the experiments in this study can be assumed to reach or approach equilibrium. The experimental temperature was measured by the NiCr–NiSi thermocouple, which is accurate to <±5 °C. Finally, the charges were quenched by turning the power off. The run products were carefully removed from the capsules and mounted in epoxy for EPMA.

2.3 | Analytical methods

Backscattered electron (BSE) images of the run products were collected using the JEOL JSM-6460LV scanning electron microscope at the State Key Laboratory of Environmental Geochemistry, Chinese Academy of Sciences. The acceleration voltage was 15 or 25 kV. The compositions of the phases in the run products were determined by the JEOL JXA-8100 electron microprobe at Chang'an University. Crystalline phases were analysed with 15 kV acceleration voltage, 2 nA sample current, and 0.5 to 2 μm beam diameter. As for the residual melt, the beam was defocused to 5 to 15 μm, and the alkaline elements were measured first to prevent the migration of Na and K (e.g., Morgan & London, 1996; Nielsen & Sigurdsson, 1981). The obtained results were corrected by a loss factor using a hydrous glass. The correction method is similar to that of Koepke, Feig, Snow, and Freise (2004).

TABLE 2 Experimental conditions and run products

Run no.	T (°C)	P (GPa)	H_2O (wt%)	Time (min)	Phase assemblage
HY01a	700	1.0	3	5,698	Hbl + Qtz + Gl
HY01b	700	1.0	5	5,698	Hbl + Qtz + Gl
HY01c	700	1.0	10	5,698	Hbl + Qtz + Gl
HY02a	850	1.0	3	6,342	Hbl + Py + Pl + Qtz + Ilm + Gl
HY02b	850	1.0	5	6,342	Py + Pl + Otz + Ilm + Gl
HY02c	850	1.0	10	6,342	Py + Pl + Ilm + Gl
HY03a	800	1.0	3	5,600	Py + Pl + Qtz + Ilm + Gl
HY03b	800	1.0	5	5,600	Hbl + Py + Pl + Qtz + Ilm + Gl
HY03c	800	1.0	10	5,600	Py + Pl + Ilm + Gl
HY04a	875	1.0	5	5,800	Hbl + Py + Pl + Ilm + Gl
HY04b	875	1.0	10	5,800	Hbl + Py + Pl + Ilm + Gl
HY04c	875	1.0	15	5,800	Py + Pl + Ilm + Gl
HY06a	875	1.5	5	4,100	Py + Alf + Ilm + Qtz + Gl
HY06b	875	1.5	10	4,100	Py + Alf + Ilm + Qtz + Gl
HY06c	875	1.5	15	4,100	Py + Alf + Ilm + Qtz + Gl
1[a]	650	0.5	3.1	4,320	Hbl + Gl
4[a]	700	0.5	5.7	4,200	Hbl + Gl
5[a]	725	0.5	3.1	4,800	Hbl + Gl
6[a]	750	0.5	3.1	4,320	Hbl + Gl
7[a]	675	0.5	6.4	4,800	Hbl + Pl + Bt + Gl
8[a]	675	1.0	7.0	4,320	Hbl + Pl + Bt + Gl

Note. Hbl = hornblende; Py = pyroxene; Pl = plagioclase; Alf = alkali feldspar; Qtz = quartz; Ilm = ilmenite; Bt = biotite; Gl = glass.

[a]The experimental runs taken from Xia et al. (2010) using the same starting material as this study.

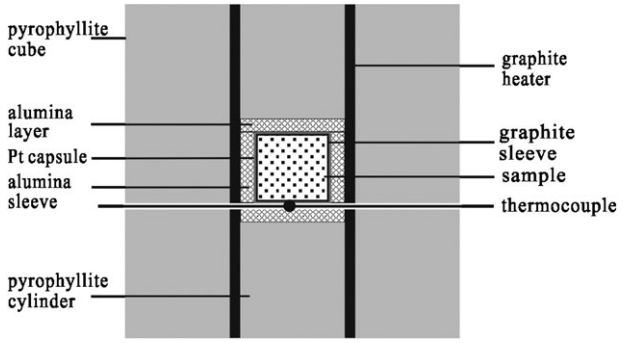

FIGURE 1 Sketch of the sample assembly used for the experiments

2.4 | Image analysis and growth rate calculation

Representative BSE images of the run products are shown in Figure 2. Experimentally crystallised plagioclases were manually outlined in BSE images using Adobe Photoshop (Brugger & Hammer, 2010; Mills & Glazner, 2013; Pupier, Duchene, & Toplis, 2008). Then, the greyscale images were converted to binary images by a thresholding process in Photoshop (Figure 2j).

Binary image analysis was conducted using the Image J software developed by National Institutes of Health (http://rsbweb.nih.gov/ij/). Areas of plagioclase and the long and short axes of best-fitting ellipses can be obtained through Image J. Crystal number density (N_A), and crystal fraction (φ) was calculated on a vesicle-free basis (Hammer, Cashman, Hoblitt, & Newman, 1999). Crystal number density (N_A) was obtained through the relation $N_A = n/A_r$ (Arzilli & Carroll, 2013; Hammer et al., 1999), where n is the number of crystals counted using Image J and A_r is the "reference area" obtained by subtracting vesicle areas from the total image area (Hammer et al., 1999). Crystal fraction (φ) was obtained through the relation $\varphi = A_c/A_r$ (Arzilli & Carroll, 2013; Hammer et al., 1999), where A_c is the area of the crystal. Then, crystal number density (N_A) and crystal fraction (φ) can be used to calculate the characteristic crystal size $S_n = (\varphi/N_A)^{1/2}$ (Brugger & Hammer, 2010; Couch, Sparks, & Carroll, 2003; Hammer & Rutherford, 2002; Hammer et al., 1999; Mills & Glazner, 2013).

Crystal growth rate was calculated using the L_{max} method (Couch, 2003; Hammer & Rutherford, 2002; Orlando et al., 2008). Ten of the largest crystals were selected for each run, and growth rates were calculated using the formula $G = (L \times W)^{0.5}/(2 \times t)$, where L is the crystal length, W is the crystal width, and t is the run time.

3 | EXPERIMENTAL RESULTS

The experimental phase assemblages from this study and previous study by Xia, Tang, and Zhu (2010) on the same starting material are listed in Table 2. The representative images of the run products are shown in Figure 2. The BSE images in this study show that the crystals tend to be larger and more euhedral at higher temperature. Thus, increasing the crystallisation temperature is conducive to the growth of large crystals. The results of microscope observation and microprobe analysis indicate that the crystallised phases in this study include the following: feldspar (Or-rich plagioclase and An-rich alkali feldspar), pyroxene (most are orthopyroxene with a few pigeonite), hornblende, quartz, and ilmenite. Compared with Xia et al. (2010), more phases such as pyroxene, An-rich alkali, and ilmenite are crystallised at higher temperature and pressure in this study. Since constructing the phase diagram is not the aim of this study, the experimental conditions are not sufficient to establish the stability field for every phase. However, some conclusions can still be drawn from Figure 3 that compares the experimental assemblages from this study with Xia et al. (2010) at similar water content condition. It can be seen from Figure 3 that (a) pyroxene crystallises mainly at high temperature and can be replaced by hornblende gradually, (b) plagioclase is mainly stable at relatively low pressure (~1.0 GPa and below), while alkali feldspar crystallises in the run at 1.5 GPa. In this study, a crystallised feldspar phase is detected in all runs, except for run 1, in which identifying whether a feldspar has crystallised or not by EPMA is difficult because of the small crystal sizes (<1 μm) in this run. Among those runs with feldspar crystallisation, plagioclase appears at 1.0 GPa (Figure 4). Owing to the relatively higher Or content in the experimental plagioclase than the natural one, it is called Or-rich plagioclase in this paper. At 1.5 GPa, the crystallised feldspars have more Or content than An content and are thus called An-rich alkali feldspars (Figure 4). In terms of composition, both Or-rich plagioclase and An-rich alkali feldspar are called ternary feldspar in this study. In Xia et al. (2010), plagioclase crystallised in two runs at the conditions of 675 °C, 0.5 and 1.0 GPa with added water of 6.4 wt% and 7.0 wt%, respectively (Table 2). However, considering the small size and thin needle-like morphology of the plagioclase in their experiments, it is likely that these crystals are quenched products. Compared with Xia et al. (2010), this study is more successful in crystallising large plagioclase crystals. The experimental products of several runs in this study contain pyroxene, a phase that rarely appears in natural granodiorites, whose stability field is restricted to high temperature (>800 °C) (Figure 3). No pyroxenes were crystallised in Xia et al. (2010) at the temperature range between 650 and 750 °C. Previous phase equilibria experiments using dioritic and granitic glasses as

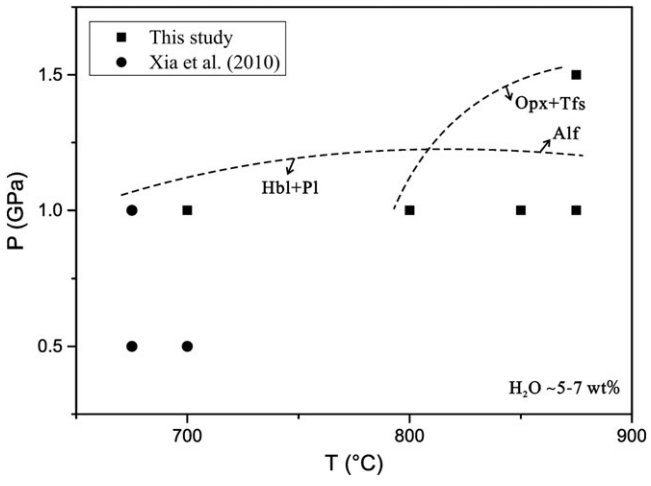

FIGURE 3 Phase diagram (pressure–temperature) for the crystallisation of the granodioritic melt using the experimental data in this study and Xia et al. (2010) at similar water content (5–7 wt%). The dashed lines are the inferred boundaries of the phases.
Hbl = hornblende; Pl = plagioclase; Alf = alkali feldspar;
Opx = orthopyroxene; Tfs = ternary feldspar (including Or-rich Pl and An-rich Alf)

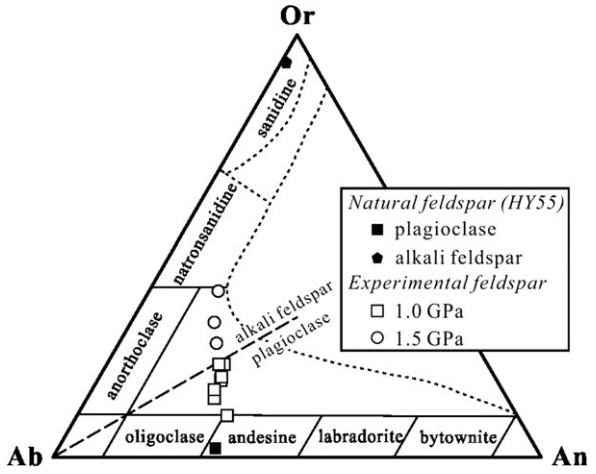

FIGURE 4 An–Ab–Or diagram for the natural and experimental feldspars

starting materials (Bogaerts et al., 2006; Klimm et al., 2003; Pietranik, Holtz, Koepke, & Puziewicz, 2009) show that pyroxene is a near-liquidus phase, which further reacts with the melt to produce hornblende when the magma is gradually cooled. The crystallisation of pyroxene is also probably affected by oxygen fugacity. The experiments of Dall'Agnol et al. (1999), whose starting material was A-type granite, revealed that the stability field of pyroxene increases as the oxygen fugacity decreases. Pyroxene crystallisation in our experiments indicates that the experiments were in a low oxygen environment, which is consistent with the fact that the oxygen fugacity was controlled by CCO buffering. Hornblende crystallised in several runs, and its composition is similar to that of the natural hornblende in the granodiorite in terms of the content of Ca, Fe, and Mg. Fe–Ti oxides appear in nearly all our experiments with high brightness in the BSE images. No Fe–Ti oxides are reported in Xia et al. (2010), which is probably due to the low experimental temperature and the lack of oxygen fugacity control in their study.

3.1 | Plagioclase and its growth rate

Plagioclases crystallised at 1.0 GPa and mainly in the temperature range of 800 to 875 °C in this study. The morphology of crystallised plagioclases is generally subhedral to euhedral (Figure 2), except for runs HY02a and HY03a in which the plagioclase boundary cannot be readily identified from BSE images due to its small crystal size. It is hence difficult to analyse the plagioclase composition accurately and to calculate the plagioclase growth rate for these two runs. With the increase of experimental undercooling, the tabular crystals gradually turn into spherulites and needles. The interiors of the crystallised plagioclases are often hollow, probably reflecting the stage of rapid cooling from above to below the liquidus (Bindeman et al., 1998).

The compositions of natural and experimental feldspars are shown in Table 3. The compositions of experimental feldspars are relatively stable, with An contents varying from 14% to 31%, mostly around 24–25%. When water is added, the An content of the experimental feldspars increases, similar to that of many previous studies (e.g., Nekvasil, 1992). All the feldspars in our experiments contain a

TABLE 3 Major element compositions (wt%) of natural and experimentally crystallised feldspars

	Starting material (HY55)		Experimentally crystallised feldspar								
Run no.	Plagioclase	Alkali feldspar	HY02b	HY02c	HY03b	HY03c	HY04a	HY04b	HY04c	HY06a	HY06b	HY06c
n	4	3	4	2	4	4	10	6	3	4	4	7
SiO_2	59.94 (0.67)	63.68 (0.50)	62.12 (1.09)	63.28 (0.23)	63.03 (2.05)	60.92 (1.90)	62.23 (1.22)	61.95 (0.95)	62.54 (0.59)	64.31 (0.77)	63.89 (0.88)	62.84 (1.82)
Al_2O_3	23.98 (0.34)	17.89 (1.00)	21.28 (0.56)	21.28 (0.06)	21.00 (1.90)	22.56 (1.50)	21.79 (1.02)	22.18 (0.67)	21.66 (0.27)	19.64 (0.75)	20.35 (1.42)	21.00 (1.36)
FeO*	0.21 (0.07)	0.12 (0.03)	0.23 (0.09)	0.29 (0.17)	0.51 (0.19)	0.58 (0.25)	0.47 (0.32)	0.33 (0.08)	0.34 (0.10)	0.34 (0.13)	0.38 (0.08)	0.22 (0.18)
CaO	6.51 (0.72)	0.10 (0.05)	4.68 (0.47)	5.07 (0.28)	4.84 (1.01)	6.05 (1.44)	4.99 (0.65)	4.92 (0.56)	4.89 (0.61)	2.82 (0.97)	3.41 (1.33)	4.06 (1.37)
Na_2O	7.38 (0.42)	0.72 (0.28)	5.98 (0.50)	6.26 (0.06)	6.40 (0.80)	6.46 (0.23)	6.19 (0.55)	6.62 (0.18)	6.07 (0.21)	5.10 (0.63)	5.80 (0.99)	5.90 (1.08)
K_2O	0.43 (0.07)	15.76 (0.65)	3.65 (0.85)	3.11 (0.29)	2.55 (1.48)	1.60 (0.82)	3.15 (0.74)	3.09 (1.04)	3.44 (0.62)	6.57 (1.89)	5.50 (2.30)	4.51 (2.23)
P_2O_5	0.01 (0.01)	0.04 (0.04)	0.11 (0.09)	0.00 (0.00)	0.05 (0.04)	0.10 (0.09)	0.05 (0.08)	0.06 (0.14)	0.14 (0.20)	0.06 (0.12)	0.03(0.04)	0.04 (0.05)
Total	98.45	98.31	98.05	99.29	98.38	98.27	98.87	99.15	99.08	98.84	99.36	98.57
An	32	1	24	25	25	31	25	24	25	14	17	20
Ab	66	6	55	56	59	60	56	58	55	47	51	53
Or	2	93	22	18	16	10	19	18	20	39	32	27

Note. *n* represents the total analytical points. Numbers in brackets are 1 SD of the oxide compositions (wt%) (similarly hereinafter).

significant amount of potassium, and their average Or contents are higher than 10%, and up to 27–39% in all the runs at 1.5 GPa. As shown in Figure 4, all the feldspars crystallised at 1.0 GPa are plagioclase, and they are called Or-rich plagioclase in this paper. At 1.5 GPa, experimental feldspars have more Or than An contents, and they are called An-rich alkali feldspar. Plagioclase with high Or contents (Or_{10-26}) also occurred in the experiments of Klimm et al. (2008), using A-type granites as the starting materials, which was believed to reflect the low CaO content (0.53 wt%) in their starting materials. Nevertheless, the CaO content in our starting material is 3.41 wt%. Thus, we contend that the low CaO content in the starting material is not the only reason for the crystallisation of Or-rich plagioclase. The occurrence of such plagioclase, as well as the An-rich alkali feldspar, is probably related to the effect of the experimental conditions. Experimental pressure can exert a significant effect on the composition of feldspars. With the increase of pressure, An contents in feldspars decrease, whereas Or contents increase (Figure 4). The Or-rich plagioclase and An-rich alkali feldspar can also be considered together as ternary feldspar. The ternary feldspar in this study can act as a buffer for keeping the total alkali relatively constant in the residual melt. The conditions and significance of ternary feldspar crystallisation will be discussed in detail in the subsequent sections.

The calculated crystal fractions (φ), number densities (N_A), characteristic crystal sizes (S_n), and growth rates (G) of the experimental feldspars (including Or-rich plagioclase at 1.0 GPa and An-rich alkali feldspar at 1.5 GPa) are listed in Table 4. The feldspar growth rates range from 1.17×10^{-8} to 2.70×10^{-8} mm/s and vary regularly with experimental temperature, pressure, and water content (Figure 5). The growth rate generally decreases with the decrease of experimental temperature, whereas elevated pressure can significantly increase the crystal growth rate. The effect of water content on plagioclase growth rate is complex. The increase of water content can initially increase the crystal growth rate. However, when water content is relatively high, the growth rate of plagioclase decreases. Swanson (1977) also observed a similar phenomenon; the maximum crystal growth rate decreases with more water, which is probably caused by the transition from diffusion-controlled growth to interface-controlled growth when water content is high. The plagioclase growth rates in this study are generally consistent with previous results (Couch, 2003; Genareau & Clarke, 2010; Larsen, 2005; Orlando et al., 2008). The plagioclase growth rates in a rhyodacitic melt determined experimentally by Larsen (2005) range between 3.5×10^{-9} and 6.57×10^{-8} mm/s, similar to our results. The experimental results of Orlando et al. (2008) show that plagioclase growth rates in a trachybasalt are 10^{-7} to 10^{-8} mm/s, which are slightly higher than our results and may be caused by the higher crystallisation temperature of trachybasaltic melt.

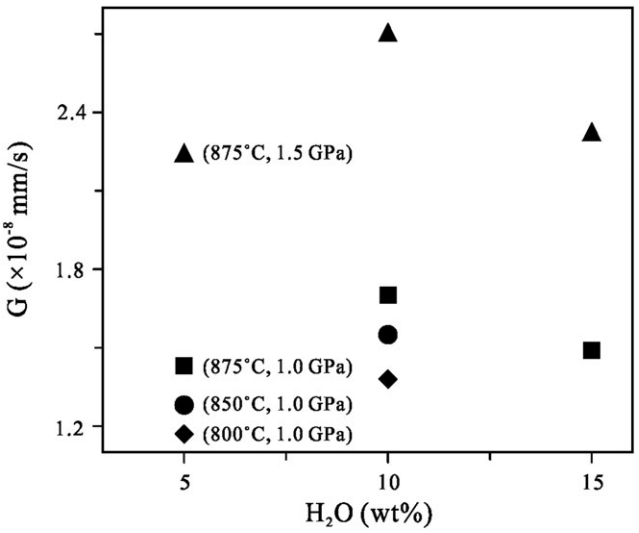

FIGURE 5 Relationship between experimental temperature, pressure, water content, and the calculated plagioclase growth rate

3.2 | Pyroxene

On the basis of their compositions (Table 5), the experimental pyroxenes are low-Ca ones (including orthopyroxenes and a few pigeonites) (Figure 6). The low-Ca pyroxenes occur in all the runs with temperature above 800 °C and are distinguished from hornblendes according to the contents of Ca, Mg, and Fe^{2+}. Generally, the experimental pyroxenes are enriched in Fe, with FeO^* contents ranging from 21.47 wt% to 31.93 wt%, and CaO contents being approximately 1 wt% to 3 wt%. The calculated Wo < 10, En = 41–49, and X_{Mg} (Mg/(Mg + Fe)) = 0.40–0.65 generally increase with the increase of water content. This is reflected, in the Wo-En-Fs diagram (Figure 6), by the gradual transition in the composition of the experimental pyroxenes,

TABLE 4 Crystal growth rates of experimentally crystallised plagioclase

Run no.	φ (vol%)	N_A(mm^{-2})	S_n (10^{-3} mm)	$(L \times W)^{0.5}$ (μm)	G (10^{-8} mm/s)
HY02b	16.40	3,004.43	7.39	7.88	1.28
HY02c	15.07	1,757.81	9.26	9.24	1.55
HY03b	7.22	2,127.90	5.83	9.71	1.17
HY03c	12.20	2,600.93	6.85	11.80	1.38
HY04a	12.54	3,398.44	6.07	9.96	1.43
HY04b	22.72	5,273.44	6.56	11.81	1.70
HY04c	29.01	10,312.50	5.30	10.37	1.49
HY06a	14.06	1,289.06	10.44	11.01	2.24
HY06b	10.03	711.80	11.87	13.30	2.70
HY06c	25.32	2,226.56	10.66	11.42	2.32

Note. φ = calculated crystal fraction; N_A = number density; S_n = characteristic crystal size; L = crystal length; W = crystal width; G = growth rate.

TABLE 5 Major element compositions (wt%) of experimentally crystallised pyroxenes

Run no.	HY02a	HY02b	HY02c	HY03a	HY03b	HY03c	HY04a	HY04b	HY04c	HY06a	HY06b	HY06c
n	4	5	4	2	2	2	4	3	6	5	6	5
SiO_2	50.50 (0.76)	49.72 (1.28)	50.35 (0.21)	52.05 (0.08)	52.69 (1.63)	51.76 (2.09)	53.33 (1.03)	52.17 (1.38)	51.66 (1.73)	48.78 (0.83)	48.85 (0.79)	49.61 (1.12)
TiO_2	0.36 (0.07)	0.33 (0.05)	0.24 (0.10)	1.17 (0.50)	0.22 (0.00)	0.76 (0.80)	0.29 (0.05)	0.37 (0.03)	0.29 (0.07)	0.28 (0.07)	0.31 (0.07)	0.48 (0.09)
Al_2O_3	2.87 (1.25)	2.32 (0.79)	1.96 (0.49)	3.47 (0.84)	3.92 (0.31)	4.56 (1.78)	2.80 (0.97)	2.35 (0.56)	2.82 (0.92)	4.24 (0.42)	3.54 (0.71)	3.63 (1.01)
FeO*	28.53 (1.07)	30.41 (0.81)	26.72 (1.10)	27.20 (2.45)	21.65 (3.78)	21.47 (5.27)	24.67 (2.43)	27.91 (0.48)	26.38 (1.60)	29.43 (1.91)	28.78 (1.04)	28.01 (1.51)
MnO	0.61 (0.11)	0.54 (0.16)	0.55 (0.15)	0.63 (0.06)	0.48 (0.20)	0.63 (0.02)	0.61 (0.08)	0.60 (0.09)	0.56 (0.10)	0.55 (0.13)	0.68 (0.15)	0.69 (0.09)
MgO	13.22 (1.29)	14.86 (1.03)	14.62 (1.17)	13.57 (1.43)	15.04 (3.40)	15.57 (2.67)	12.89 (1.02)	15.83 (0.32)	14.24 (1.09)	13.63 (1.32)	14.43 (1.24)	14.93 (0.65)
CaO	2.32 (1.26)	1.72 (1.05)	3.44 (1.79)	1.68 (0.24)	3.32 (0.14)	3.51 (0.50)	4.45 (0.56)	1.87 (0.05)	3.13 (1.30)	1.32 (0.25)	1.78 (0.20)	1.69 (0.28)
Na_2O	0.21 (0.10)	0.10 (0.10)	0.20 (0.14)	0.82 (0.63)	0.50 (0.38)	0.37 (0.20)	0.50 (0.28)	0.09 (0.07)	0.33 (0.18)	0.13 (0.09)	0.12 (0.10)	0.20 (0.05)
K_2O	0.21 (0.20)	0.12 (0.09)	0.04 (0.02)	0.38 (0.28)	0.68 (0.54)	0.94 (0.00)	0.45 (0.50)	0.16 (0.10)	0.31 (0.23)	0.05 (0.04)	0.05 (0.03)	0.07 (0.03)
Total	98.84	100.12	98.13	100.98	98.49	99.56	99.87	101.35	99.71	98.40	98.55	99.33
Wo	5	4	8	4	7	8	10	4	7	3	4	4
En	43	44	46	45	51	51	43	47	45	44	44	46
Fs	52	52	47	51	42	41	47	49	48	53	52	50
X_{Mg}	0.45	0.47	0.49	0.47	0.55	0.56	0.48	0.50	0.49	0.45	0.47	0.49

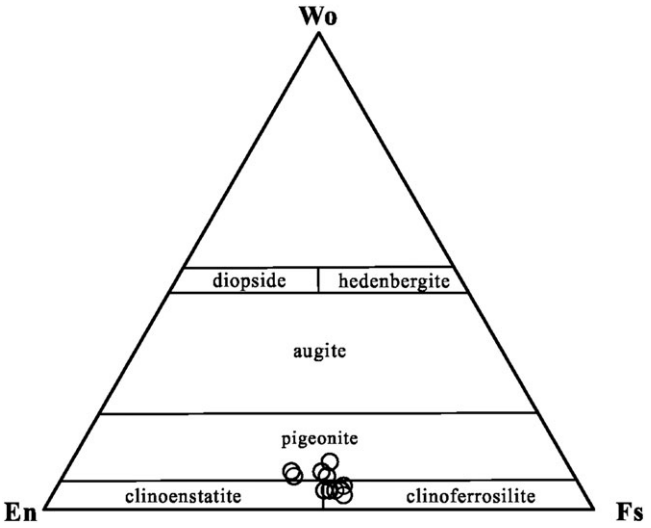

FIGURE 6 Wo–En–Fs diagram for the experimental pyroxenes

which pass from Fe-richer orthopyroxenes to Mg-richer pigeonites. All the crystallised pyroxenes have a certain amount of Al_2O_3 (approximately 3 wt%), which is slightly higher than that of natural pyroxenes but is still consistent with previous experimentally crystallised pyroxenes (Pietranik et al., 2009). This finding can be probably related to the activity of Al_2O_3 in the melt (Bogaerts et al., 2006).

3.3 | Hornblende

The compositions of hornblende in natural rocks and experiments are shown in Table 6. In terms of the contents of Ca, Fe, and Mg, the experimental hornblendes are similar to the natural hornblendes. The CaO contents of experimental hornblendes are in the range of 7 wt% to 12 wt%, the MgO contents in the range of 11 wt% to 12 wt%, and the FeO* contents in the range of 17 wt% to 22 wt%. $(Fe^{2+} + Fe^{3+})/(Fe^{2+} + Fe^{3+} + Mg^{2+})$ ratios lie between 0.39 and 0.50. In the structural formula, $(Na + K)_A < 0.5$, $Ca_A < 0.5$, and $Ca_B > 1.5$ indicating that hornblende belongs to magnesiohornblende in the calcic amphiboles category (Leake et al., 1997). The Al contents in the natural and experimental hornblendes are relatively low, further indicating that hornblendes are probably the product of reactions between pyroxenes and melt during the crystallisation of magma. Using the same method for calculating plagioclase growth rates, we also determined the hornblende growth rates in run HY03b. The obtained result is 8.93×10^{-9} mm/s, similar to the result (3.47×10^{-9} to 1.85×10^{-8} mm/s) of Browne, Gardner, and Larsen (2003).

3.4 | Ilmenite

Fe–Ti oxides occur in most of the runs, with a bladed or granular morphology, and should be a near-liquidus phase according to previous phase equilibria studies (e.g., Dall'Agnol et al., 1999). The compositions of Fe–Ti oxides acquired by EPMA may have been contaminated by melt because of their small sizes. In general, the TiO_2 content (approximately 40 wt%) is slightly higher than the FeO* content (approximately 35 wt%), indicating that the molar ratio of these two

TABLE 6 Major element compositions (wt%) of natural and experimentally crystallised hornblendes

	Starting material	Experimentally crystallised hornblende			
Run no.	Hbl	HY02a	HY03b	HY04a	HY04b
n	5	1	3	3	2
SiO_2	50.81 (2.02)	49.54	50.51 (1.33)	49.67 (1.60)	50.16 (2.13)
TiO_2	0.59 (0.30)	0.67	0.84 (0.59)	0.60 (0.10)	0.68 (0.14)
Al_2O_3	4.12 (1.37)	8.59	8.11 (0.49)	3.77 (0.56)	5.44 (1.34)
FeO*	17.02 (1.02)	14.85	16.50 (1.50)	21.93 (0.24)	18.28 (2.20)
MnO	0.53 (0.04)	0.53	0.45 (0.11)	0.67 (0.02)	0.49 (0.06)
MgO	12.54 (0.77)	13.15	12.45 (2.12)	12.13 (0.57)	10.75 (0.05)
CaO	10.74 (0.60)	9.43	7.16 (1.83)	9.35 (0.81)	11.17 (2.48)
Na_2O	0.89 (0.38)	0.92	1.06 (0.46)	0.36 (0.25)	0.61 (0.04)
K_2O	0.36 (0.14)	0.26	0.40 (0.33)	0.11 (0.16)	0.47 (0.29)
Total	97.59	97.94	97.46	98.59	98.04
$(Ca + Na)_B$	1.79	1.59	1.41	1.36	1.74
Na_B	0.09	0.13	0.30	0.00	0.09
$(Na + K)_A$	0.23	0.18	0.37	0.12	0.26
Fe/(Fe + Mg)	0.43	0.39	0.43	0.50	0.49

molecules is approximate 1:1. Therefore, the Fe–Ti oxides in this study are mainly ilmenites.

3.5 | Residual melt

The major element compositions of the residual melts after progressive crystallisation are shown in Table 7 and Figure 7. SiO_2 contents are in the range of 71.3 wt% to 73.9 wt%. The total alkali contents are relatively high (8 wt% to 10 wt%), whereas CaO and MgO contents are low (most <1.80 wt% and <0.35 wt%, respectively), with relatively high FeO^*/MgO ratios (most >7). These characteristics are similar to those of A-type granites (Eby, 1990).

As shown in Figure 7a, the residual melts have obviously higher SiO_2 and K_2O, but lower CaO and Al_2O_3 contents than the starting material, suggesting that plagioclase is an important fractionating mineral from the granodioritic melt. This is further displayed in Figure 7b, showing a linear increase of SiO_2 and K_2O in the residue melts, as well as a linear decrease of CaO and Na_2O, with the increase of the plagioclase crystal fractions. In addition, it is clearly shown from the experimental conditions (Table 2) and the compositions (Table 7) of runs HY04a-c and HY06a-c that increasing pressure reduces the K_2O contents in the residual melts under the same temperature and water content.

4 | DISCUSSION

4.1 | The optimal conditions for plagioclase crystallisation in granodioritic melts

Determining the crystallisation conditions of plagioclase in granodioritic melts is necessary to better understand the magma evolution processes and elemental partitioning behaviour between granodioritic melt and crystallised plagioclase. In this study, identifiable plagioclase crystallised at 800 to 875 °C, 1.0 GPa conditions. Compared with the natural plagioclase, all the experimental plagioclases have much higher Or contents (Figure 4), which could be due to the fact that experimental pressure is higher than the actual crystallisation pressure of the magma. According to the Al-in-hornblende geobarometer proposed by Anderson and Smith (1995), the estimated crystallisation pressure for granodiorite in East Junggar is approximately 60 to 140 MPa (Su, 2007), which is significantly lower than the experimental pressures in this study. As mentioned above, the Or contents in feldspar increase with increasing pressure. Thus, low pressure condition (at least less than 1.0 GPa) is beneficial to the crystallisation of plagioclase with less Or content from granodioritic melts.

According to the BSE images of run products (Figure 2), the crystallised plagioclase at 875 °C is relatively large and euhedral. Compared with Xia et al. (2010) at 650 to 750 °C, the crystallised plagioclase in our experiments is larger and more euhedral. As mentioned above, the plagioclases in Xia et al. (2010) are mostly thin needles, indicating that the plagioclase may be a quenched product. Therefore, a temperature of 875 °C or higher may be suitable to grow large plagioclase crystals in granodioritic melt.

Water content can also significantly affect the crystallisation of plagioclase in the aspect of crystallisation temperature, composition, and crystal size. It should be noted that the exact amount of water in the melts after experiments in this study was not determined due to the lack of hydrous standard glasses with known water content and the occurrence of many crystals that make it difficult to determine the water content in residual melts using methods such as infrared spectroscopy. However, all the experimental charges should be water undersaturated because of the high pressure of this study. According to the water solubility model in the granitic system proposed by Holtz, Johannes, Tamic, and Behrens (2001), water solubility in granitic melt increases significantly with pressure. They formulated an empirical equation to calculate the water solubility: H_2O solubility (wt%) = $2.859 \times 10^{-2} \times P - 1.495 \times 10^{-3} \times P^{1.5} + 2.702 \times 10^{-5} \times P^2 + 0.257 \times P^{0.5}$, where P is the pressure in MPa. From this equation, the water solubility at 1.0 and 1.5 GPa would be 16.5 wt% and 26.8 wt%, respectively, higher than the added water content in our experiments. As a result, all the added water can be assumed to be

TABLE 7 Major element compositions (wt%) of experimental residual melts

Run no.	HY02a	HY02b	HY02c	HY03a	HY03b	HY03c	HY04a	HY04b	HY04c	HY06a	HY06b	HY06c
n	3	3	2	2	3	4	8	6	6	4	4	5
SiO_2	73.75 (1.59)	71.46 (0.15)	73.30 (0.03)	72.90 (1.85)	73.16 (1.90)	71.29 (1.21)	72.52 (0.97)	72.87 (0.46)	73.88 (0.89)	72.89 (0.52)	72.77 (0.46)	73.10 (0.79)
TiO_2	0.33 (0.08)	0.40 (0.11)	0.35 (0.05)	0.22 (0.01)	0.20 (0.20)	0.29 (0.14)	0.38 (0.09)	0.42 (0.09)	0.39 (0.11)	0.37 (0.08)	0.41 (0.05)	0.32 (0.12)
Al_2O_3	13.59 (0.08)	14.11 (0.36)	13.38 (0.25)	14.01 (0.85)	13.88 (1.19)	14.93 (0.45)	13.74 (0.47)	13.90 (0.26)	13.64 (0.41)	14.25 (0.27)	14.13 (0.54)	14.42 (0.15)
FeO*	2.09 (0.23)	1.98 (0.23)	2.03 (0.14)	2.08 (0.73)	1.65 (0.14)	2.04 (0.89)	2.39 (0.84)	1.95 (0.10)	2.01 (0.29)	2.44 (0.36)	2.32 (0.18)	2.15 (0.16)
MnO	0.07 (0.12)	0.03 (0.05)	0.05 (0.03)	0.05 (0.04)	0.07 (0.07)	0.10 (0.07)	0.06 (0.09)	0.08 (0.04)	0.03 (0.05)	0.05 (0.06)	0.05 (0.06)	0.03 (0.02)
MgO	0.27 (0.12)	0.27 (0.03)	0.27 (0.04)	0.38 (0.06)	0.32 (0.24)	0.29 (0.21)	0.52 (0.44)	0.28 (0.11)	0.27 (0.12)	0.26 (0.06)	0.30 (0.11)	0.29 (0.01)
CaO	1.41 (0.19)	1.48 (0.07)	1.48 (0.09)	1.70 (0.31)	1.95 (0.18)	2.32 (0.12)	1.57 (0.27)	1.37 (0.09)	1.31 (0.04)	1.53 (0.19)	1.61 (0.18)	1.48 (0.07)
Na_2O	3.13 (0.41)	4.11 (0.15)	3.74 (0.28)	3.20 (0.27)	4.08 (0.27)	4.60 (0.67)	3.14 (0.31)	3.28 (0.18)	3.22 (0.30)	3.44 (0.13)	3.37 (0.12)	3.23 (0.14)
K_2O	5.18 (1.05)	5.98 (0.07)	5.16 (0.31)	5.18 (0.76)	4.52 (0.38)	3.98 (0.31)	5.47 (0.59)	5.72 (0.19)	5.10 (0.50)	4.54 (0.50)	4.69 (0.40)	4.83 (0.82)
P_2O_5	0.19 (0.26)	0.18 (0.12)	0.22 (0.00)	0.31 (0.11)	0.17 (0.12)	0.20 (0.08)	0.20 (0.14)	0.14 (0.13)	0.15 (0.13)	0.23 (0.23)	0.35 (0.22)	0.13 (0.18)
Total	94.47	94.41	96.07	96.55	95.53	94.29	96.25	96.52	94.81	93.73	94.08	92.94

Note. The individual oxide contents are normalised to 100 wt%, whereas the total is the result before normalisation.

solubilised in the experimental residual melts, and the melts are all water undersaturated. Usually, with increase of water content in the melt, the crystallisation temperature of plagioclase decreases (Klimm et al., 2003; Martel et al., 1999; Takagi et al., 2005). High water content may also suppress the crystallisation of plagioclase (Danyushevsky, 2001; Muntener, Kelemen, & Grove, 2001). Danyushevsky (2001) investigated the effect of H_2O on the fractionation of MORB and BABB, showing that the crystallisation of plagioclase is suppressed by adding a small amount of water. Muntener et al. (2001) experimentally investigated the role of H_2O during the crystallisation of primitive arc magmas under uppermost mantle conditions, implying that increase of water content changes the crystallisation sequence, and high water contents can suppress plagioclase, leading to the crystallisation of amphibole and garnet. On the basis of the BSE images (Figure 2), plagioclases are larger and more euhedral in runs with approximately 10 wt% water than those with approximately 15 wt% water. This is consistent with previous studies that high water content is not favourable to the crystallisation of plagioclase. However, the crystallisation of plagioclase in runs with approximately 10 wt% water is even better (larger crystals and higher growth rates) than runs with approximately 5 wt% water, which seems to contradict the above results. This is probably related to the combined effects of water on the diffusion of chemical components and on the plagioclase stability field. On the one hand, high water content can suppress the crystallisation of plagioclase as discussed above; on the other hand, increasing water content is conducive to the diffusion of chemical components needed for the crystallisation of plagioclase, as can be seen from the increase of plagioclase growth rate when water content is increased from 5 wt% to 10 wt%. Therefore, as long as diffusion is no longer a limiting factor for the crystal growth, lower water content is favourable to the crystallisation of plagioclase in the granodioritic melt.

In summary, for the temperature range of 700 to 875 °C, pressure of 1.0 and 1.5 GPa, and water being undersaturated in the melt investigated in this study, the optimal condition for plagioclase to crystallise in the granodioritic melt is approximately 875 °C, 1.0 GPa and relatively low water content (~10 wt% in this study). This conclusion may apply to other granodioritic melts whose compositions are similar to HY55 (A/CNK < 1, A/NK > 1) and can be a good reference for crystallising large plagioclase crystals in order to further study the trace element partitioning behaviour in granodioritic melts in the future.

4.2 | Crystallisation and significance of ternary feldspar

The Or-rich plagioclase crystallised at 1.0 GPa and the An-rich alkali feldspar crystallised at 1.5 GPa in this study can be called ternary feldspar in terms of composition ($Ab_{47\text{-}60}An_{14\text{-}31}Or_{10\text{–}39}$). Ternary feldspars also occurred in the previous studies (Hammer & Rutherford, 2002; Klimm et al., 2008; Litvinovsky, Steele, & Wickham, 2000). Hammer and Rutherford (2002) conducted decompression-induced crystallisation experiments on a dacitic melt from Pinatubo volcano, the experimental product of which includes ternary feldspar ($Ab_{69}An_{11}Or_{20}$). They believed that the occurrence of ternary feldspar reflects the low $(Ca/K)_{pl}/(Ca/K)_{glass}$ between feldspar and melt under

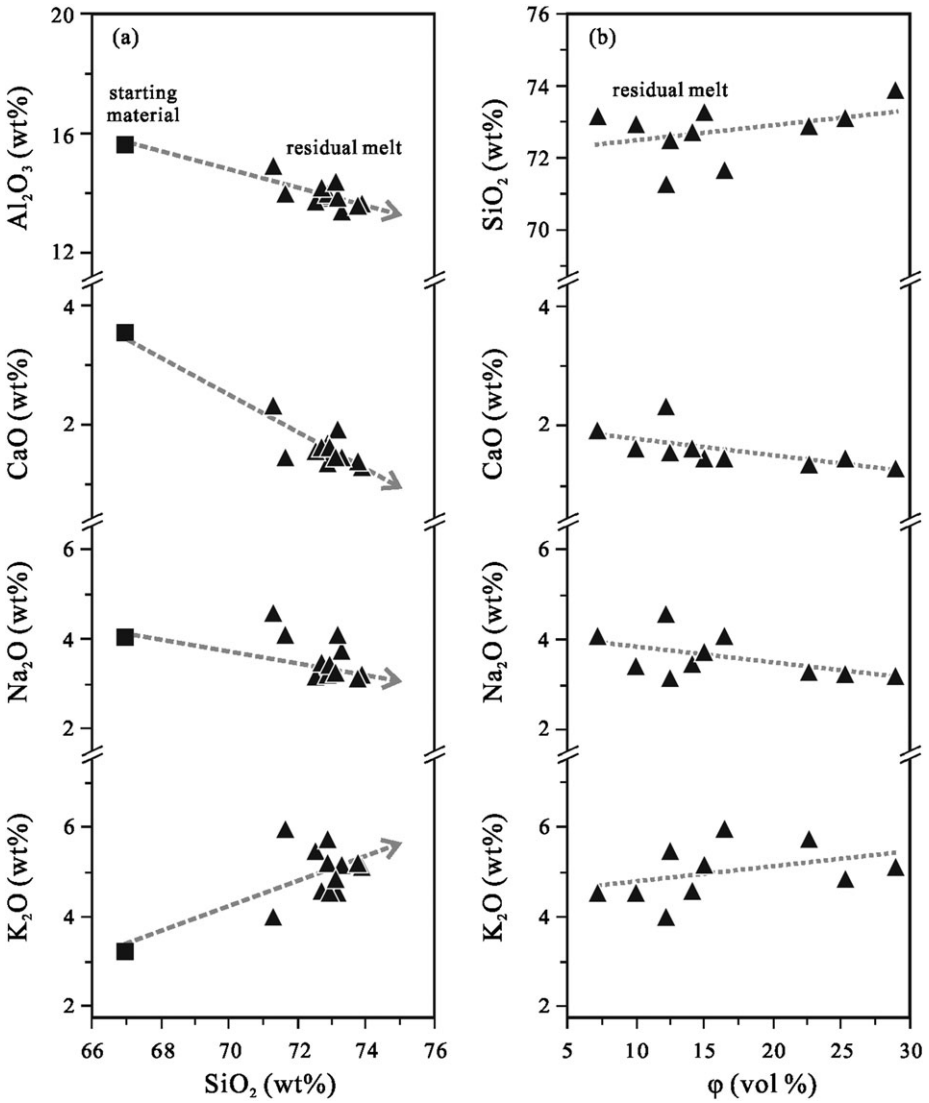

FIGURE 7 Major elements (Al_2O_3, CaO, Na_2O, and K_2O) versus SiO_2 in residual melts and comparison with the starting material (a), and major elements versus the calculated plagioclase crystal fraction (b)

experimental conditions. In our experiments, $(Ca/K)_{pl}/(Ca/K)_{glass}$ is 1.04 to 5.67, which is significantly lower than 8.69 of natural rock, and is 1.04 to 2.18 at 1.5 GPa, which is lower than that of 2.55 to 5.67 at 1.0 GPa. These results indicate that partitioning of Ca/K between feldspar and melt is distinctly affected by crystallisation pressure. Thus, the crystallisation of ternary feldspar is probably due to the lower efficiency of the Ca/K partitioning between feldspar and melt under high pressure conditions.

Litvinovsky et al. (2000) performed partial melting experiments on charnockite with similar compositions to HY55 at high pressures (1.5–2.5 GPa). Euhedral and homogeneous ternary feldspars also occur in their experiments. The melt produced by partial melting remains granitic even when the degree of partial melting reaches approximately 60 vol.% because of the buffering role of ternary feldspar that usually forms at the beginning of the melting, along with garnet and pyroxene. Litvinovsky et al. (2000) insisted that the ternary feldspars were formed by plagioclase and potassium feldspars via melting reactions and that ternary feldspars play a significant role in buffering the partial melt composition. In our experiments, the Na_2O content of the residual melt at 1.5 GPa is slightly higher than at 1.0 GPa; however, the K_2O content is the opposite (Table 7). Correspondingly, the ternary feldspars at 1.5 GPa are richer in K and poorer in Na than at 1.0 GPa (Figure 4). These complementary trends between ternary feldspar and residual melt indicate that ternary feldspars play a role in maintaining a basically constant total alkali content of residual melt. In conclusion, ternary feldspars crystallise with the increase of pressure and ensure that the total alkali contents of residual melt remain relatively constant at different pressures.

4.3 | Petrogenesis of the A-type granite in East Junggar

A-type granite is an important granite type widely distributed all over the world and related to some specific geological settings (e.g., anorogenic settings) and processes. It is highly enriched in SiO_2 and alkali, with high FeO^*/MgO ratio and low CaO content. Currently, the petrogenesis of A-type granites is still in debate. Many researchers have proposed different genetic models to

explain the origin of A-type granites, including (a) high fractionation of mantle-derived basic magmas (Han et al., 1997; Turner, Foden, & Morrison, 1992); (b) partial melting of melt-depleted rocks in the lower crust (Clemens, Holloway, & White, 1986; Collins, Beams, White, & Chappell, 1982); (c) partial melting of crustal rocks (tonalite and granodiorite) (Creaser, Price, & Wormald, 1991; Patiño Douce, 1997); (d) interactions between mantle-derived magmas and crustal rocks (Kerr & Fryer, 1993); (e) partial melting of charnockite and anorthosite in the lower crust (Frost, Frost, Bell, & Chamberlain, 2002; Litvinovsky et al., 2000); and (f) fractionation of intermediate-acidic magmas (Hergt et al., 2007; Jiang et al., 2009; Klimm et al., 2003; Su et al., 2008).

Thus far, only a few experimental studies on the formation of A-type granites by partial melting of crustal rocks have been conducted (Dall'Agnol et al., 1999; Litvinovsky et al., 2000; Patiño Douce, 1997; Skjerlie & Johnston, 1992). However, the experimental evidence of fractionation of intermediate-acidic magmas accounting for the petrogenesis of A-type granite is scarce. Using A-type granites of different evolution stages from Lachlan Fold Belt, Australia, as the starting materials, Klimm et al. (2003, 2008) experimentally constrained the conditions for the formation of A-type granites. They suggested that the variations in composition of the A-type granites in that region were a result of fractional crystallisation. Given that their starting materials consisted of less-evolved A-type granite, their experimental results can only reveal that fractional crystallisation is the main reason for the compositional variety of A-type granites but cannot account as to whether fractionation of melts with intermediate–acidic composition (e.g., I-type granodioritic melt) can form melt with A-type characteristics or not.

Our experimental results show that fractional crystallisation of I-type granodioritic melt at high pressure in the deep crust is a possible process accounting for the petrogenesis of A-type granites. After minerals, such as plagioclase (or ternary feldspar) and pyroxene, crystallise, the composition of residual melt displays characteristics of typical A-type granite (enrichment in SiO_2 and total alkali, depletion in CaO and MgO, with high FeO^*/MgO ratios) (Figure 7). In the plots of $FeO^*/(FeO^* + MgO)$ versus SiO_2 and $Na_2O + K_2O$–CaO versus SiO_2, the compositions of the residual melts plot into the range of typical A-type granites and partly coincide with those of the A-type granites from East Junggar (Figure 8). Therefore, in terms of major element compositions, the A-type granites in East Junggar may be formed by the fractional crystallisation of the I-type granodioritic magma at high pressure.

From our experimental results, with granodioritic glass as the starting material, the major element compositions of the residual melt after fractionation of Pl, Opx, and Hbl can be estimated by mass balance calculation. Given that the crystallised plagioclase in Run 03 has similar An content to that in natural rock (An_{26-31} and An_{29}, respectively), Pl, Opx, and Hbl in Run 03 are selected as the fractionally crystallised minerals in the calculation. The calculated result is shown in Table 8. After crystallisation of 40.2 wt% plagioclase, 6.3 wt% orthopyroxene, and 6.3 wt% hornblende, the granodioritic melt will leave a residual melt with similar compositions to that of the sample HY42, a representative A-type granite from East Junggar. Although a little difference exists in the Na_2O and K_2O contents, which may be caused by the variations in plagioclase composition, the contents of total alkali roughly remain the same.

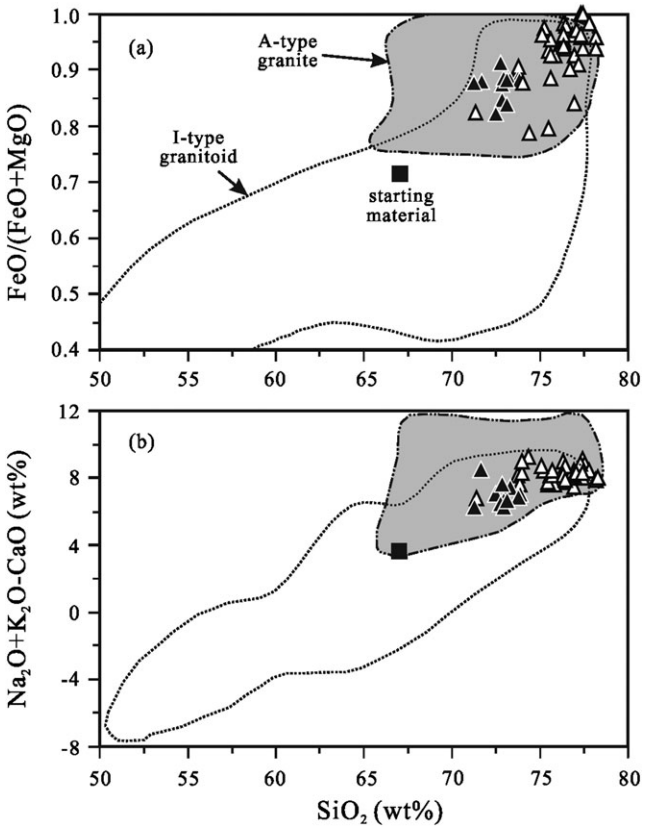

FIGURE 8 $FeO^*/(FeO^* + MgO)$ and ($Na_2O + K_2O$–CaO) versus SiO_2 diagrams for the residual melt (▲) after fractional crystallisation of the granodioritic melt at studied temperatures, pressures, and water contents and its comparison with A-type granite (Δ) from East Junggar of Xinjiang (data cited from Su et al., 2007; Su, 2007). The regions for I-type and A-type granites are based on the data range for Lachlan Fold Belt, Australia (after Frost et al., 2001)

TABLE 8 Calculated residual melt compositions (wt%) after fractional crystallisation of the initial melt by 40.2 wt% Pl, 6.3 wt% Opx, and 6.3 wt% Hbl

	HY55	Pl	Opx	Hbl	Calculated	HY42
SiO_2	67.02	61.83	50.56	51.75	75.60	75.60
TiO_2	0.54	0.08	1.33	0.86	0.78	0.51
Al_2O_3	15.62	22.90	3.32	8.31	12.01	11.59
FeO*	4.22	0.59	26.05	16.90	2.73	2.60
MnO	0.07	0.02	0.62	0.46	0.00	0.16
MgO	1.69	0.15	13.76	12.75	0.00	0.19
CaO	3.52	6.14	3.17	7.33	0.83	0.68
Na_2O	3.99	6.55	0.22	1.08	2.69	4.06
K_2O	3.18	1.62	0.96	0.41	5.17	4.36
P_2O_5	0.14	0.11	0.00	0.14	0.19	0.23

Note. Contents of the oxides are normalised to 100 wt%. Data of the initial melt (HY55) and the representative A-type granite in East Junggar (HY42) are from Su (2007).

On the basis of the mass balance calculation from major element compositions, the trace element compositions during the fractional

crystallisation of the I-type granodioritic melt can be simulated. Two fractional crystallisation models were employed, namely, the Rayleigh crystallisation model ($C_L^i = C_0^i \times F^{(D-1)}$) and the equilibrium crystallisation model ($C_L^i = C_0^i/[F + (1 - F) \times D]$), where C_0^i is the concentration of trace element *i* in the initial melt, C_L^i is the concentration of trace element *i* in the residual melt, *D* is the total partitioning coefficient, and *F* is the fraction of residual melt (47.2 wt%). The calculated results are shown in Table 9 and Figure 9.

As shown in Figure 9, the Rayleigh model and the equilibrium crystallisation model have similar rare earth element (REE) patterns. However, the REE pattern from the Rayleigh model displays more pronounced and similar negative Eu anomaly to the A-type granites from East Junggar, implying that the Rayleigh model is closer to the actual crystallisation. In the classification diagrams of $(Na_2O + K_2O)/CaO$ versus 10,000 Ga/Al and Zr + Nb + Ce + Y (Figure 10) proposed by Whalen, Currie, and Chappell (1987) to discriminate A-type granite from other granite types, the calculated compositions of the residual melt fall into the region of A-type granite. As a consequence, the results of trace element modelling also indicate that the fractional crystallisation of the I-type granodioritic melt at high pressure can lead to the formation of the A-type granites in East Junggar. In consideration of the study of Jiang et al. (2009) that shows that the parental magma of a Mesozoic granite with A-type characteristics from the North China Craton is likely to be I-type granitoids, we suggest that the fractional crystallisation of I-type granitoids in the deep crust may be one of the processes for the origin of A-type granites worldwide.

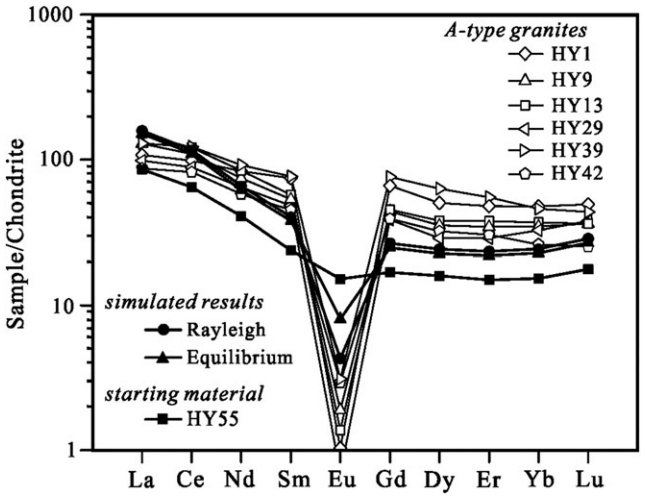

FIGURE 9 Comparison between calculated rare earth element patterns and those of granodiorite and A-type granites from East Junggar (chondrite values are from Sun and McDonough, 1989)

4.4 | Timescale of the crystallisation and differentiation of the granodioritic magma in East Junggar

The timescale of magma crystallisation and differentiation is one of the key parameters to understand the evolution and dynamics of magmas. In general, one can distinguish several timescales related to the magma evolution by fractional crystallisation (Hawkesworth et al., 2000): the time taken to build a magma chamber, the time taken for a differentiated magma to evolve from its parental source, and the time taken for the magma to emplace. Understanding these timescales can definitely provide us a dynamic picture of the magmatic processes. In this study, the experimentally determined crystal growth rates were used to make constraints on the timescale of the crystallisation and differentiation of the granodioritic magma in East Junggar. As discussed above, the A-type granites in East Junggar were probably formed by the fractionation of the granodioritic magma at depth; here, we estimate the timescale for this differentiation process (time taken for the A-type granitic magma to evolve from the I-type granodioritic magma).

TABLE 9 Partitioning coefficients used in the calculation and the calculated trace element concentrations

	Partitioning coefficient			Starting material	Calculated concentration (ppm)		A-type granite from East Junggar (ppm)					
	Pl	Opx	Hbl	HY55	Rayleigh	Equilibrium	HY1	HY9	HY13	HY29	HY39	HY42
La	0.38	0.11	0.35	20.3	37.52	35.74	25.5	30.5	36.1	23.4	30.7	20.6
Ce	0.27	0.15	1.52	39.5	71.28	67.54	60.4	67.1	74.0	54.4	75.1	50.2
Nd	0.203	0.22	4.26	19.1	30.79	28.76	39.0	34.8	39.2	30.2	43.0	27.1
Sm	0.097	0.017	3.99	3.63	6.18	5.80	11.4	8.17	8.76	7.39	11.7	6.89
Eu	5.417	2.85	5.14	0.88	0.25	0.47	0.06	0.11	0.08	0.04	0.18	0.17
Gd	0.125	0.027	5.48	3.47	5.46	5.09	13.6	9.04	9.29	7.93	15.6	8.05
Dy	0.064	0.46	6.2	4.05	6.14	5.73	12.8	8.95	9.64	7.33	16.0	8.16
Er	0.055	0.072	5.94	2.47	3.87	3.61	7.93	5.7	6.24	4.76	9.13	5.04
Yb	0.049	0.86	4.89	2.60	4.14	3.86	8.10	5.91	6.28	5.55	7.79	4.43
Lu	0.046	0.9	4.53	0.45	0.73	0.68	1.25	0.92	0.92	0.96	1.11	0.64
Ga	1.5	0.32	2.42	15.4	18.23	17.47	29.0	22.0	23.4	29.7	24.8	22.4
Zr	0.2	0.11	0.5	127	246.1	237.5	246	541	456	257	268	103
Nb	0.57	0.64	0.2	5.60	9.60	9.02	22.7	11.2	14.8	8.25	9.93	5.47
Y	0.32	0.755	2.46	20.5	33.9	32.0	83.7	52.0	58.0	38.6	88.2	47.0

Note. Partitioning coefficients for rare earth elements are quoted from Rollinson (1993) for dacitic and rhyolitic systems; the partitioning coefficients for Ga, Zr, and Y are obtained from the GERM Partitioning Coefficient Database (https://earthref.org/KDD/). The trace element data of the A-type granites from East Junggar are from Su (2007). See text for the calculation in detail.

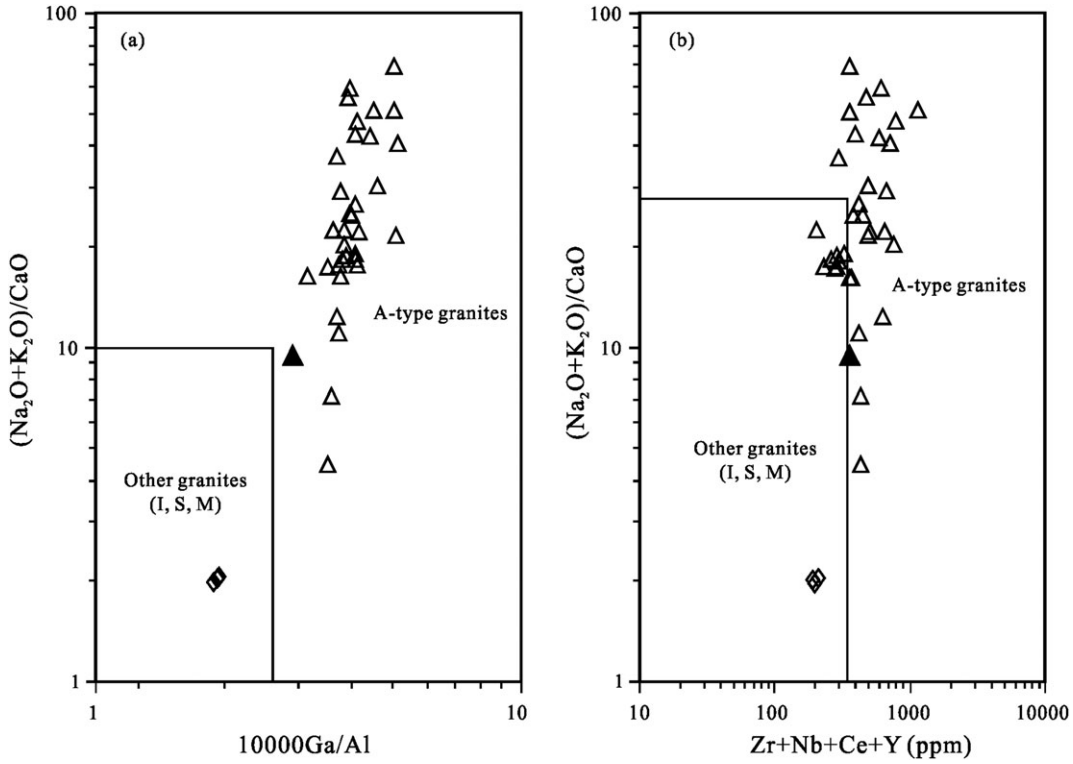

FIGURE 10 ($Na_2O + K_2O$)/CaO versus 10,000 Ga/Al (a) and (Zr + Nb + Ce + Y) (b) diagrams for discriminating A-type granite from other granite types (after Whalen et al., 1987). The I-type granodiorites (◊) and the A-type granites (Δ) from East Junggar, NW China, are shown for comparison (data cited from Su et al., 2007; Su, 2007; Yang et al., 2011). The residual melt (▲) after fractional crystallisation of the granodioritic melt is from the element calculations (Tables 8 and 9)

The growth time of plagioclase is usually used to determine the timescales of the crystallisation and emplacement of the plutonic intrusion (e.g., Cheng, Zeng, Ren, Wang, & Luo, 2014) because of its extensive appearance in igneous rocks and wide range of crystallisation conditions. In our proposed model, the A-type granites in East Junggar were formed by the differentiation of granodioritic magma dominated by the crystallisation of plagioclase. Therefore, the crystallisation time of plagioclase in granodioritic magma can provide a basic estimation of the differentiation timescale of the A-type magma evolved from the I-type granodioritic magma. In order to better constrain this timescale, the growth rate of hornblende is also considered in the calculation. By comparing the experimentally determined crystal growth rate with the crystal size in natural granodiorites, the crystallisation time of the crystals can be calculated. On the basis of the growth rate of plagioclase shown in Table 4 and Figure 5, it may increase linearly with the increase of pressure (the growth rates at 1.5 GPa are approximately 1.5 times faster than those at 1.0 GPa). For simplification, the equation $G_0 = G_1 \times P_0/P_1$ was used to calculate the growth rates under emplacement pressure conditions, where G_0 and G_1 are the crystal growth rates at pressure P_0 and P_1, respectively. Temperature also has an effect on crystal growth rates. From our experimental results, the empirical equations describing the relationship between temperature and crystal growth rate can be obtained by linear fitting of the plagioclase growth data at different temperatures for water contents of 5 wt% and 10 wt% (Figure 11). According to the estimation of Su (2007), the granodiorite intrusion in East Junggar emplaced at conditions of 60 to 140 MPa (average of 100 MPa) and 700 to 728 °C (average of

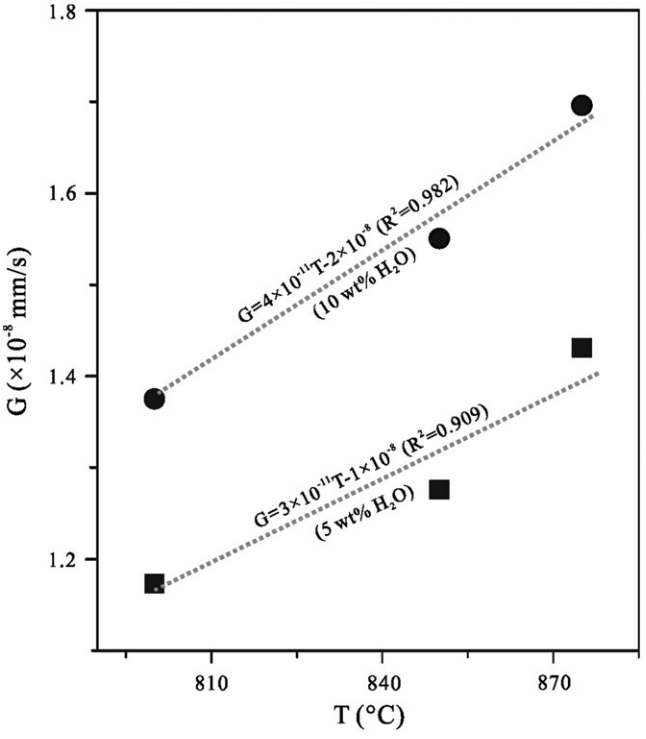

FIGURE 11 Relationship between temperature and crystal growth rate at 1.0 GPa

714°C). On the basis of the aforementioned relationship between pressure, temperature, and crystal growth rates, the calculated growth rates at 100 MPa and 714°C are 8.56×10^{-10} to

1.14×10^{-9} mm/s for plagioclase and 7.97×10^{-10} mm/s for hornblende.

Hammer (2008) and Orlando et al. (2008) have demonstrated that the crystal growth rates decrease with crystallisation time. As a first-order approximation, the plagioclase and hornblende growth rates are assumed to decrease linearly with time during the crystallisation of the magma, which allows the evaluation of crystal size (L) as a function of time (t). Thus, from $G = G_0 - kt$, where G_0 is the crystal growth rate at the onset of crystallisation, which can be replaced by our experimental results because the experimental duration can be neglected when compared with natural crystallisation time, and k is the decay constant, we can derive the following equation.

$$L = \int_0^t (G_0 - kt)dt = G_0 t - kt^2/2 \quad (1)$$

Consequently, as long as the mineral sizes in natural rocks are known, the crystallisation time can be calculated using Equation 1. The average sizes of relatively large plagioclases and hornblendes in natural rocks were used to estimate the crystallisation timescale of the granodioritic magma. The average sizes are approximately 1.5 mm for plagioclase and approximately 0.5 mm for hornblendes. The calculated results are $k = 9.1 \times 10^{-20}$ to 4.3×10^{-19} mm/s^2, t = 92 to 536 years. Therefore, the timescale of granodioritic magma crystallisation and differentiation is estimated to be several hundred years. This estimation is a first-order approximation with several assumptions: (a) Crystal growth rates increase linearly with pressure and temperature, and (b) growth rates decrease linearly with crystallisation time. In the natural crystallisation processes, magma cooling rate, composition change of melt due to the crystallisation of minerals, thermal instability, and magma contamination, all can affect the crystallisation kinetics of magma. Despite these uncertainties, the estimation using crystal growth rate is in excellent agreement with the result by a numerical model discussed below, as well as falls into the typical timescale range (10^2 to 10^4 years) of the crystallisation of granitic plutons as reviewed by Petford, Cruden, McCaffrey, and Vigneresse (2000), which validates its effectiveness in estimating the timescale of magma crystallisation and differentiation.

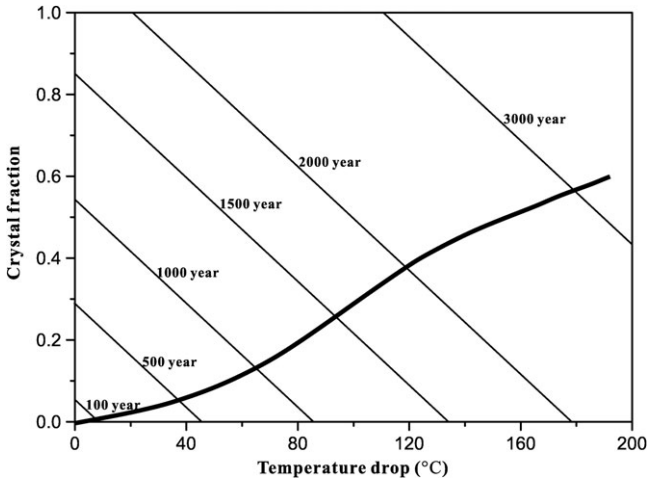

FIGURE 12 The contours calculated using Equation 2 show the number of years required to crystallise a mass fraction of φ and drop the temperature by ΔT below the liquidus for magma in a 10 km^3 chamber losing heat at 100 MW. The black curve is the calculated crystallisation history of a synthetic melt with similar composition to that of the granodiorite on the basis of the experimental result of Brugger et al. (2003)

A simple heat balance model for predicting the timescales of magma differentiation was proposed by Hawkesworth et al. (2000) and had been applied to study the timescale of the emplacement and crystallisation of the Panzhihua gabbroic intrusion in SW China by Cheng et al. (2014). The model considers cooling of a chemically closed magmatic system. The maximum amount of magmatic cooling can be estimated by equating the geothermal power output P to the thermal energy lost from a fixed volume of magma (V) divided by the cooling time t_{cool}:

$$P = V\rho\,(c\Delta T + \Phi L)/t_{cool} \quad (2)$$

where ρ is the magma density in kilogramme per cubic metre, c is the specific heat capacity, L is the latent heat of crystallisation, ΔT is the temperature drop, and Φ is the fraction of crystals grown over this temperature range (Cheng et al., 2014; Hawkesworth et al., 2000). The representative values for a rhyolite with similar composition to the granodiorite were used in this study (ρ = 2200 kg/m^3, $c = 1.6 \times 10^3$ J/kg per K, $L = 2.5 \times 10^5$ J/kg) (Hawkesworth et al., 2000). On the basis of the geological mapping, the granodiorite intrusion is ~10 km^3 in volume. For this volume size, the rate at which the thermal energy is lost from magma chambers maintains geothermal power outputs about 100 MW (Hawkesworth et al., 2000). Then, the timescale of the magma crystallisation can be calculated by using various combinations of ΔT and φ according to Equation 2. The calculated results are illustrated in Figure 12. Also shown is the path of increasing crystal fraction with the lowering of temperature for a synthetic silicate melt with generally similar composition to the granodiorite in this study on the basis of the phase equilibria experimental results by Brugger et al. (2003). According to our mass balance calculation results above, when the total crystal fraction (Pl 40.2 wt% + Opx 6.3 wt% + Hbl 6.3 wt%) exceeds 50 wt%, the residue melt shows A-type characteristics. As can be seen from Figure 12, the granodioritic magma reaches 50 wt% crystallisation after less than 1,000 years, which means that the timescale of the crystal fractionation in the granodioritic magma is hundreds of years, consistent with the result obtained by the crystal growth rate above. Consequently, it had taken hundreds of years for the crystallisation and differentiation of the granodioritic magma to generate the A-type granites in East Junggar.

5 | CONCLUSIONS

Crystallisation experiments were performed on a natural granodioritic glass from East Junggar, NW China, at conditions of 700 to 875 °C, 1.0 and 1.5 GPa, and various water contents. The followings are the main conclusions of this study:

1. The main crystallised phases in the granodioritic melt under experimental conditions are Or-rich plagioclase, An-rich alkali feldspar, pyroxene, hornblende, and Fe–Ti oxides. The Fe–Ti

oxides and pyroxene are near-liquidus phases. With the decrease of experimental temperature, plagioclase and hornblende crystallise. Pyroxene is not observed in the natural granodiorite, implying that it may have reacted with the melt to produce hornblende.

2. The composition and morphology of experimental plagioclase vary systematically with experimental conditions. As the temperature decreases, the morphology of plagioclase changes from tabular crystals to spherulites and needles. An increase of experimental pressure leads to a decrease of An content and an increase of Or content in the experimental plagioclase. The optimal conditions for plagioclase to crystallise in this granodioritic melt are 875 °C, 1.0 GPa and with ~10 wt% water. At high pressure, ternary feldspar may crystallise because of the low efficiency of Ca/K partitioning between feldspar and melt. Ternary feldspar plays a role in keeping the total alkali content of the melts relatively stable.
3. The mass balance calculation and trace element modelling on the basis of our experimental results show that the A-type granites in East Junggar can be formed by the fractional crystallisation of the I-type granodioritic magma at high pressure, in which plagioclase is the dominantly differentiated mineral.
4. Experimentally determined plagioclase growth rates range from 1.17×10^{-8} to 2.70×10^{-8} mm/s and vary regularly with the experimental conditions. According to the relationship between crystal growth rate and crystal size in natural granodiorite, the timescale for the crystallisation and differentiation of the granodioritic magma in East Junggar is estimated to be hundreds of years, consistent with the results from a numerical model calculation, indicating that the A-type granites in East Junggar can be formed within hundreds of years by the fractional crystallisation of the granodioritic magma.

ACKNOWLEDGEMENTS

This work was financially supported by the Strategic Priority Research Programme (B) of the Chinese Academy of Sciences (XDB 18010401) and the National Natural Science Foundation of China (Grant 41172071). We are grateful to Professor Patrizia Fiannacca and one anonymous reviewer for their constructive comments that substantially improve the manuscript. M. Liu is appreciated for the assistance on the EPMA analysis. We thank W. Zhou, M. Wang, and C. Zhu for their help on the experiments.

CONFLICT OF INTEREST

The authors declare no conflict of interests.

REFERENCES

Aigner-Torres, M., Blundy, J., Ulmer, P., & Pettke, T. (2007). Laser ablation ICPMS study of trace element partitioning between plagioclase and basaltic melts: An experimental approach. *Contributions to Mineralogy and Petrology*, *153*, 647–667 https://doi.org/10.1007/s00410-006-0168-2.

Anderson, J. L., & Smith, D. R. (1995). The effects of temperature and fO_2 on the Al-in-hornblende barometer. *American Mineralogist*, *80*, 549–559.

Andersson, U. B., & Eklund, O. (1994). Cellular plagioclase intergrowths as a result of crystal-magma mixing in the Proterozoic Aland rapakivi batholiths, SW Finland. *Contributions to Mineralogy and Petrology*, *117*, 124–136.

Arzilli, F., & Carroll, M. R. (2013). Crystallization kinetics of alkali feldspars in cooling and decompression-induced crystallization experiments in trachytic melt. *Contributions to Mineralogy and Petrology*, *166*, 1011–1027 https://doi.org/10.1007/s00410-013-0906-1

Bindeman, I. N., & Davis, A. M. (2000). Trace element partitioning between plagioclase and melt: Investigation of dopant influence on partition behavior. *Geochimica et Cosmochimica Acta*, *64*, 2863–2878 https://doi.org/10.1016/S0016-7037(00)00389-6

Bindeman, I. N., Davis, A. M., & Drake, M. J. (1998). Ion microprobe study of plagioclase-basalt partition experiments at natural concentration levels of trace element. *Geochimica et Cosmochimica Acta*, *62*, 1175–1193 https://doi.org/10.1016/S0016-7037(98)00047-7

Bogaerts, M., Scaillet, B., & Auwera, J. V. (2006). Phase equilibria of the Lyngdal granodiorite (Norway): Implications for the origin of metaluminous ferroan granitoids. *Journal of Petrology*, *47*, 2405–2431 https://doi.org/10.1093/petrology/egl049

Browne, B. L., Gardner, J. E., Larsen, J. 2003. Amphibole reaction rims in response to decompression compared to heating: An experimental approach. *American Geophysical Union, Fall Meeting* #V12A-0551.

Brugger, C. R., & Hammer, J. E. (2010). Crystal size distribution analysis of plagioclase in experimentally decompressed hydrous rhyodacite magma. *Earth and Planetary Science Letters*, *300*, 246–254 https://doi.org/10.1016/j.epsl.2010.09.046

Brugger, C. R., Johnston, A. D., & Cashman, K. V. (2003). Phase relations in silicic systems at one-atmosphere pressure. *Contributions to Mineralogy and Petrology*, *146*, 356–369 https://doi.org/10.1007/s00410-003-0503-9

Cabane, H., Laporte, D., & Provost, A. (2005). An experimental study of Ostwald ripening of olivine and plagioclase in silicate metls: Implications for the growth and size of crystal in magmas. *Contributions to Mineralogy and Petrology*, *150*, 37–53 https://doi.org/10.1007/s00410-005-0002-2

Cheng, L., Zeng, L., Ren, Z., Wang, Y., & Luo, Z. (2014). Timescale of emplacement of the Panzhihua gabbroic layered intrusion recorded in giant plagioclase at Sichuan Province, SW China. *Lithos*, *204*, 203–219 https://doi.org/10.1016/j.lithos.2014.04.017

Clemens, J. D., Holloway, J. R., & White, A. J. R. (1986). Origin of an A-type granite: Experimental constraints. *American Mineralogist*, *71*, 317–324.

Collins, W. J., Beams, S. D., White, A. J. R., & Chappell, B. W. (1982). Nature and origin of A-type granites with particular reference to southeastern Australia. *Contributions to Mineralogy and Petrology*, *80*, 189–200.

Corrigan, G. M. (1982). The crystal morphology of plagioclase feldspar produced during isothermal supercooling and constant rate cooling experiments. *Mineralogical Magazine*, *46*, 433–439.

Couch, S. (2003). Experimental investigation of crystallization kinetics in a haplogranite system. *American Mineralogist*, *88*, 1471–1485 https://doi.org/10.2138/am-2003-1011.

Couch, S., Sparks, R. S. J., & Carroll, M. R. (2003). The kinetics of degassing-induced crystallization at Soufrière Hills volcano, Montserrat. *Journal of Petrology*, *44*, 1477–1502 https://doi.org/10.1093/petrology/44.8.1477

Creaser, R. A., Price, R. C., & Wormald, R. J. (1991). A-type granites revisited: Assessment of a residual-source modal. *Geology*, *19*, 163–166.

Dall'Agnol, R., Scaillet, B., & Pichavant, M. (1999). An experimental study of a lower Proterozoic A-type granite from the eastern Amazonian craton, Brazil. *Journal of Petrology*, *40*, 1673–1698 https://doi.org/10.1093/petroj/40.11.1673

Danyushevsky, L. V. (2001). The effect of small amount of H_2O on crystallization of mid-ocean ridge and backarc basin magmas. *Journal of Volcanology and Geothermal Research*, *110*, 265–280 https://doi.org/10.1016/S0377-0273(01)00213-X

Eby, G. N. (1990). The A-type granitoids: A review of their occurrence and chemical characteristics and speculations on their petrogenesis. *Lithos*, *26*, 115–134.

Frost, B. R., Barnes, C. G., Collins, W. J., Arculus, R. J., Ellis, D. J., & Frost, C. D. (2001). A geochemical classification for granitic rocks. *Journal of Petrology*, *42*, 2033–2048 https://doi.org/10.1093/petrology/42.11.2033

Frost, C. D., Frost, B. R., Bell, J. M., & Chamberlain, K. R. (2002). The relationship between A-type granites and residual magmas from anorthosite: Evidence from the northern Sherman batholith, Laramie Mountains, Wyoming, USA. *Precambrian Research*, *119*, 45–71 https://doi.org/10.1016/S0301-9268(02)00117-1

Genareau, K., & Clarke, A. B. (2010). In situ measurements of plagioclase growth using SIMS depth profiles of $^{7}Li/^{30}Si$: A means to acquire crystallization rates during short-during decompression events. *American Mineralogist*, *95*, 592–601 https://doi.org/10.2138/am.2010.3292

Gibb, F. G. F. (1974). Supercooling and the crystallization of plagioclase from a basaltic magma. *Mineralogical Magazine*, *39*, 641–653.

Grove, T. L., Baker, M. B., & Kinzler, R. J. (1984). Coupled CaAl-NaSi diffusion in plagioclase feldspar: Experiments and application to cooling rate speedometry. *Geochimica et Cosmochimica Acta*, *48*, 2113–2121.

Hammer, J. E. (2008). Experimental studies of the kinetics and energetics of magma crystallization. *Reviews in Mineralogy and Geochemistry*, *69*, 9–59 https://doi.org/10.2138/rmg.2008.69.2

Hammer, J. E., & Rutherford, M. J. (2002). An experimental study of kinetics of decompression-induced crystallization in silicic melt. *Journal of Geophysical Research*, *107*, B1 https://doi.org/10.1029/2001JB000281

Hammer, J. E., Cashman, K. V., Hoblitt, R. P., & Newman, S. (1999). Degassing and microlite crystallization during pre-climactic events of the 1991 eruption of Mt. Pinatubo, Philippines. *Bulletin of Volcanology*, *60*, 355–380.

Han, B., Wang, S., Jahn, B., Hong, D., Kagami, H., & Sun, Y. (1997). Depleted-mantle source for the Ulungur River A-type granites from North Xinjiang, China: Geochemistry and Nd–Sr isotopic evidence, and implications for Phanerozoic crustal growth. *Chemical Geology*, *138*, 135–159 https://doi.org/10.1016/S0009-2541(97)00003-X

Hawkesworth, C. J., Blake, S., Evans, P., Hughes, R., Macdonald, R., Thomas, L. E., … Zellmer, G. (2000). Time scales of crystal fractionation in magma chambers – integrating physical, isotopic and geochemical perspectives. *Journal of Petrology*, *41*, 991–1006 https://doi.org/10.1093/petrology/41.7.991.

Hergt, J., Woodhead, J., & Schofield, A. (2007). A-type magmatism in the Western Lachlan Fold Belt? A study of granites and rhyolites from the Grampians region, Western Victoria. *Lithos*, *97*, 122–139 https://doi.org/10.1016/j.lithos.2006.12.008

Holtz, F., Johannes, W., Tamic, N., & Behrens, H. (2001). Maximum and minimum water contents of granitic melts generated in the crust: A reevaluation and implications. *Lithos*, *56*, 1–14 https://doi.org/10.1016/S0024-4937(00)00056-6

Housh, T. B., & Luhr, J. F. (1991). Plagioclase-melt equilibria in hydrous systems. *American Mineralogist*, *76*, 477–492.

Jiang, N., Zhang, S., Zhou, W., & Liu, Y. (2009). Origin of a Mesozoic granite with A-type characteristics from North China craton: Highly fractionated from I-type magmas? *Contributions to Mineralogy and Petrology*, *158*, 113–130 https://doi.org/10.1007/s00410-008-0373-2.

Kerr, A., & Fryer, B. J. (1993). Nd isotope evidence for crust-mantle interaction in the generation of A-type granitoid suites in Labrador, Canada. *Chemical Geology*, *104*, 39–60.

Klimm, K., Holtz, F., Johannes, W., & King, P. L. (2003). Fractionation of metaluminous A-type granites: An experimental study of the Wangrah Suite, Lachlan Fold Belt, Australia. *Precambrian Research*, *124*, 327–341 https://doi.org/10.1016/S0301-9268(03)00092-5

Klimm, K., Holtz, F., & King, P. L. (2008). Fractionation vs. magma mixing in the Wangrah Suite A-type granites, Lachlan Fold Belt, Australia: Experimental constraints. *Lithos*, *102*, 415–434 https://doi.org/10.1016/j.lithos.2007.07.018

Koepke, J., Feig, S. T., Snow, J., & Freise, M. (2004). Petrogenesis of oceanic plagiogranites by partial melting of gabbros: An experimental study. *Contributions to Mineralogy and Petrology*, *146*, 414–432 https://doi.org/10.1007/s00410-003-0511-9

Larsen, J. F. (2005). Experimental study of plagioclase rim growth around anorthite seed crystals in rhyodacitic melt. *American Mineralogist*, *90*, 417–427 https://doi.org/10.2138/am.2005.1456

Leake, B. E., Woolley, A. R., Arps, C. S., Birch, W. D., Gilbert, M. C., Grice, J. D., … Youzhi, G. (1997). Nomenclature of amphiboles: Report of the subcommittee on amphiboles of the international mineralogical association commission on new minerals and mineral names. *Canadian Mineralogist*, *35*, 219–246.

Litvinovsky, B. A., Steele, I. M., & Wickham, S. M. (2000). Silicic magma formation in overthickened crust: Melting of charnockite and leucogranite at 15, 20 and 25 kbar. *Journal of Petrology*, *41*(5), 717–734 https://doi.org/10.1093/petrology/41.5.717

Lofgren, G. (1974). An experimental study of plagioclase crystal morphology: Isothermal crystallization. *American Journal of Science*, *274*, 1243–1273.

Loomis, T. P., & Welber, P. W. (1982). Crystallization processes in the Rocky Hill granodiorite pluton, California: An interpretation based on compositional zoning of plagioclase. *Contributions to Mineralogy and Petrology*, *81*, 230–239.

Martel, C., Pichavant, M., Holtz, F., Scaillet, B., Bourdier, J., & Traineau, H. (1999). Effect of fO_2 and H_2O on andesite phase relations between 2 and 4 kbar. *Journal of Geophysical Research*, *104*, 29453–29470 https://doi.org/10.1029/1999JB900191

Mills, R. D., & Glazner, A. F. (2013). Experimental study on the effects of temperature cycling on coarsening of plagioclase and olivine in an alkali basalt. *Contributions to Mineralogy and Petrology*, *166*, 97–111 https://doi.org/10.1007/s00410-013-0867-4

Mollo, S., Putirka, K., Iezzi, G., Del Gaudio, P., & Scarlato, P. (2011). Plagioclase-melt (dis)equilibrium due to cooling dynamics: Implications for thermometry, barometry and hygrometry. *Lithos*, *125*, 221–235 https://doi.org/10.1016/j.lithos.2011.02.008

Morgan, G. B., & London, D. (1996). Optimizing the electron microprobe analysis of hydrous alkali aluminosilicate glasses. *American Mineralogist*, *81*, 1176–1185.

Morse, S. (1984). Cation diffusion in plagioclase feldspar. *Science*, *225*, 504–505.

Muncill, G. E., & Lasaga, A. C. (1987). Crystal-growth kinetics of plagioclase in igneous systems: One atmosphere experiments and application of a simplified growth model. *American Mineralogist*, *72*, 299–311.

Muncill, G. E., & Lasaga, A. C. (1988). Crystal-growth kinetics of plagioclase in igneous systems: Isothermal H_2O-saturated experiments and extension of a growth model to complex silicate melts. *American Mineralogist*, *73*, 982–992.

Muntener, O., Kelemen, P. B., & Grove, T. L. (2001). The role of H_2O during crystallization of primitive arc magmas under uppermost mantle conditions and genesis of igneous pyroxenites: An experimental study. *Contributions to Mineralogy and Petrology*, *141*, 643–658 https://doi.org/10.1007/s004100100266

Nekvasil, H. (1992). Feldspar crystallization in felsic magmas: A review. *Transactions of the Royal Society of Edinburgh: Earth Sciences*, *83*, 399–407.

Nielsen, C. H., & Sigurdsson, H. (1981). Quantitative methods for electron microprobe analysis of sodium in natural and synthetic glasses. *American Mineralogist*, *66*, 547–552.

Orlando, A., D'Orazio, M., Armienti, P., & Borrini, D. (2008). Experimental determination of plagioclase and clinopyroxene crystal growth rate in an anhydrous trachybasalt from Mt Etna (Italy). *European Journal of Mineralogy*, *20*, 653–664 https://doi.org/10.1127/0935-1221/2008/0020-1841

Panjasawatwong, Y., Danyushevsky, L. V., Crawford, A. J., & Harris, K. L. (1995). An experimental study of the effects of melt composition on plagioclase-melt equilibria at 5 and 10 kbar: Implications for the origin

of magmatic high-An plagioclase. *Contributions to Mineralogy and Petrology*, *118*, 420–432.

Patiño Douce, A. E. (1997). Generation of metaluminous A-type granites by low-pressure melting of calc-alkaline granitoids. *Geology*, *25*, 743–746.

Petford, N., Cruden, A. R., McCaffrey, K. J. W., & Vigneresse, J. L. (2000). Granite magma formation, transport and emplacement in the Earth's crust. *Nature*, *408*, 669–673 https://doi.org/10.1038/35047000

Pietranik, A., Holtz, F., Koepke, J., & Puziewicz, J. (2009). Crystallization of quartz dioritic magmas at 2 and 1 kbar: Experiments results. *Mineralogy and Petrology*, *97*, 1–21 https://doi.org/10.1007/s00710-009-0070-5

Prouteau, G., & Scaillet, B. (2003). Experimental constraints on the origin of the 1991 Pinatubo dacite. *Journal of Petrology*, *44*(12), 2203–2241.

Pupier, E., Duchene, S., & Toplis, M. J. (2008). Experimental quantification of plagioclase crystal size distribution during cooling of a basaltic liquid. *Contributions to Mineralogy and Petrology*, *150*, 555–570 https://doi.org/10.1007/s00410-007-0258-9

Rollinson, H. R. 1993. Using geochemical data: Evaluation, presentation, interpretation. Longman Scientific and Technical, 108–111.

Rudnick, R. L., & Gao, S. (2014). The composition of the continental crust. In *Treatise on geochemistry* (2nd ed., Vol. 4) (pp. 1–51). Oxford: Elsevier-Pergamon.

Scaillet, B., & Evans, B. W. (1999). The 15 June 1991 eruption of Mount Pinatubo. I. Phase equilibria and pre-eruption P–T–fO_2–fH_2O conditions of the dacite magma. *Journal of Petrology*, *40*(3), 381–411.

Simakin, A. G., & Salova, T. P. (2004). Plagioclase crystallization from a Hawaiitic melt in experiments and in a volcanic conduit. *Petrology*, *1*, 98–109.

Sisson, T. W., & Grove, T. L. (1993). Experimental investigations of the role of H_2O in calc-alkaline differentiation and subduction zone magmatism. *Contributions to Mineralogy and Petrology*, *113*, 143–166.

Skjerlie, K. P., & Johnston, A. D. (1992). Vapor-absent melting at 10 kbar of a biotite- and amphibole-bearing tonalitic gneiss: Implications for the generation of A-type granites. *Geology*, *20*, 263–266.

Su, Y. 2007. Geochronological and geochemical study on the A-type granites from Junggar, Xinjiang. Ph.D. Thesis, University of Chinese Academy of Sciences (in Chinese with English abstract).

Su, Y., Tang, H., Sylvester, P. J., Liu, C., Qu, W., Hou, G., & Cong, F. (2007). Petrogenesis of Karamaili alkaline A-type granites from East Junggar, Xinjiang (NW China) and their relationship with tin mineralization. *Geochemical Journal*, *41*, 341–357.

Su, Y., Tang, H., & Cong, F. (2008). Zircon U-Pb age and petrogenesis of the Huangyangshan alkaline granite body in East Junggar, Xinjiang. *Acta Mineralogica Sinica*, *28*(2), 117–126 (in Chinese with English abstract).

Sun, S., & McDonough, M. F. (1989). Chemical and isotopic systematics of oceanic basalts: Implications for mantle composition and processe. *Geological Society, London, Special Publications*, *42*, 313–345.

Swanson, S. E. (1977). Relation of nucleation and crystal-growth rate to the development of granitic textures. *American Mineralogist*, *62*, 966–978.

Takagi, D., Sato, H., & Nakagawa, M. (2005). Experimental study of a low-alkali tholeiite at 1-5 kbar: Optimal conditions for the crystallization of high-An plagioclase in hydrous arc tholeiite. *Contributions to Mineralogy and Petrology*, *149*, 527–540 https://doi.org/10.1007/s00410-005-0666-7

Tang, H., Qu, W., Su, Y., & Cong, F. (2007). Genetic connection of Sareshike tin deposit with the alkaline A-type granites of Sabei body in Xinjiang: Constraint from isotopic ages. *Acta Petrologica Sinica*, *23*(08), 1989–1997 (in Chinese with English abstract).

Turner, S. P., Foden, J. D., & Morrison, R. S. (1992). Derivation of some A-type magmas by fractionation of basaltic magma: An example from the Padthaway Ridge, South Australia. *Lithos*, *28*, 151–179.

Whalen, J. B., Currie, K. L., & Chappell, B. W. (1987). A-type granites: Geochemical characteristics, discrimination and petrogenesis. *Contributions to Mineralogy and Petrology*, *95*, 407–419.

Wilke, M., & Behrens, H. (1999). The dependence of the partitioning of iron and europium between plagioclase and hydrous tonalitic melt on oxygen fugacity. *Contributions to Mineralogy and Petrology*, *137*, 102–114.

Xia, W., Tang, H., & Zhu, C. (2010). Experimental study on crystallization of plagioclases from a granodioritic melt at high temperature and high pressure. *Journal of Mineralogy and Petrology*, *30*(1), 22–25 (in Chinese with English abstract).

Yang, G., Li, Y., Wu, H., Zhong, X., Yang, B., Yan, C., … Si, G. (2011). Geochronological and geochemical constrains on petrogenesis of the Huangyangshan A-type granite from the East Junggar, Xinjiang, NW China. *Journal of Asian Earth Sciences*, *40*, 722–736.

Zhao, Z., Wang, Z., Zou, T., & Masude, A. (1996). Study on petrogenesis of alkali-rich intrusive rocks of Ulungur, Xinjiang. *Geochemica*, *25*(3), 205–220 (in Chinese with English abstract).

How to cite this article: Xu M, Tang H. Plagioclase crystallisation in a granodioritic melt and its petrogenetic implications for the origin of the A-type granite in East Junggar, NW China. *Geological Journal*. 2018;53:929–946. https://doi.org/10.1002/gj.2935